POLITECNICO DI TORINO

Master of Science in Petroleum and Mining Engineering

Design and analysis of tunnel cross-passage opening: 3D finite difference analysis vs 3D shell-spring approach

Supervisor:

Dr: Daniele Martinelle

Co.Supervisor:

Eng: Floria Vincenza

Candidate:

Hosameldin Khogali Suliman Hag Hamid

October-2023

Acknowledgements

A special thanks is addressed to Dr Daniele Martinelli, for last year's teachings, and in particular for the availability and patience shown in supporting me in this master's thesis process; but that's not all, as having given me the opportunity to carry out the curricular internship at the engineering company Pini Group Spa was an extraordinary experience to say the least and one that I will keep precious for the future.

This allowed me to come into direct contact with a high-level reality on the international scene, but no less important, also from a personal point of view. In a nutshell, an environment that has always made me feel at ease, finding people very willing to provide an opinion or advice whenever needed, but also showing how the role of "superior" constitutes a title, rather than an attitude, thus helping to create a comfortable working environment.

In this regard, thanks go to the engineering company Pini Group, for allowing me to continue my thesis work. Still with reference to Pini Group Spa, thanks are more than due to the engineer Floria Vincenza for Co-supervising me during the thesis period and for giving me the opportunity to carry out my thesis in the company.

Finally, a very special thanks goes to the engineers Luca Bertetto, Salvador Safina and Carlo Chiesa for the precious and decisive support provided, in the form of advice and more.

Executive Summary

In TBM tunnelling, the connection between the mainline tunnel and cross-passages typically occurs once the tunnel drive is complete. During this temporary construction phase, the precast segmental lining is being opened by removing segments in the opening area. In order to continuously support and stabilise the remaining segment rings, segments have to be equipped with load-transfer elements to ensure the deviation of the interrupted annular forces, hence (Steel segments or frames). Finite difference analysis and shell-spring approach are two widely adopted methods to quantify the induced loads in a tunnel lining: for a typical sequential ring, without any openings. This study assesses the effectiveness of utilizing the three-dimensional lagrangian finite-volume software (FLAC3D) and the structural finite element software (SAP2000) in evaluating cross-passage opening-induced stress redistribution occurring in the segmental lining.

For this purpose, member forces were derived using each method based on a case where a cross-passage was being constructed between two bored tunnels. The study found that the predicted lining member forces from the FDM model align with those of the SSM before the construction of the cross-passage opening. This was extended for the creation of the segmental lining opening on both models, prior to advancing into cross-passage excavation. The critical areas concerning the load capacity of the segmental lining opening were identified at the segmental linings positioned at the lateral sides of the opening. Additionally, it was noted that resulting member forces on the lining in the two models do not lie in agreement anymore, as this was attributed to stresses redistribution around the opening within the 3D difference model. In due course, a simplistic solution was proposed to put both models in agreement and results were plotted. Moreover, longitudinal and circumferential joints between rings and segments were incorporated in both models, as the presence of these joints showed significant influence on the load transfer mechanism between the opened ring and the adjacent fully enclosed ring. Finally, temporary steel support system was installed in both models and resulting member forces were derived.

To conclude, the study shows that for a similar case, one can use more simplistic 3D shell-spring models to examine the lining response rather than carrying out complex 3D finite difference models, and that the design of a temporary support system can also be conducted relatively easily and precisely.

List of figures

List of Tables

Table of Contents

1. Introduction

The increasing use of rail and road tunnels has led to a rise in tunnel accidents and emergencies over the past few decades, which are often more perilous than open-air road incidents (Ribeiro E 2006). Escaping from underground tunnels during emergencies poses significant challenges (Mashimo 2002). To address this issue, the construction of cross-passages at regular intervals has become a vital aspect of building railway and road tunnels (Lee T-H 2017). Cross-passages, situated between twin-tube TBM tunnels or between a TBM tunnel and a shaft structure, provide a safe means of egress during emergencies and serve various functions during normal tunnel operation and maintenance. Consequently, cross-passages have become a crucial component in tunnelling projects worldwide. Typically, the construction of tunnel cross-passages occurs towards the project's conclusion to avoid disruption to main tunnel excavation activities. However, delays in completing cross-passages can potentially postpone the overall project delivery. Constructing these cross-passages presents complex technical challenges, including support for excavation, excavation profile management, and dealing with existing bored tunnel linings (Kuyt J 2015). These challenges carry a significant schedule and cost risk in tunnelling projects. Implementing adequate support measures during cross-passage construction is essential to minimize these risks. To achieve this, both geotechnical and structural techniques must be integrated into the cross-passage design.

Modern Tunnel Boring Machines (TBMs) facilitate the construction of bored tunnels using precast segmental concrete linings installed behind the TBM as it advances. This process involves cutting open the segmental lining or installing special opening segments to create cross-passage openings from the main tunnel. In a single-pass lining system, the segmental lining serves as both initial ground support during excavation and final tunnel support. However, creating an opening for a cross-passage alters the simple lining behaviour, leading to increased complexity. The lack of structural connection between adjacent segments' reinforcing steel further complicates this behaviour. The abrupt change in ring sectional dimensions results in high-stress concentrations around the opening, causing significant stress redistribution of internal forces and moments within the lining. Additionally, the opening's creation reduces the stiffness of the segmental ring, potentially causing excessive deformations. The load borne by the tunnel lining from which segments are removed is transferred to the adjacent fully enclosed rings, necessitating strengthening of the tunnel lining. To design this strengthening work effectively, it is essential to quantify the stress concentrations and ring distortions resulting from the opening.

Despite the prevalence of cross-passages in modern tunnelling projects, there is limited literature on this topic. Past researchers, such as Klappers et al. and Zhang et al., have highlighted the lack of

understanding of the structural mechanisms of tunnel openings. Li et al. have observed that much of the available literature in this field focuses on lining design and construction from an industrial perspective rather than approaching the problem scientifically. Due to the limited understanding of the loading mechanism's behaviour and the associated risks, design methods for cross-passage construction often incorporate significant conservatism, resulting in potentially excessive support usage. Optimizing the support amount can offer significant benefits in terms of project time and cost, but achieving this requires a better understanding of load development, emphasizing the need for effective design methods that lead to efficient and less problematic solutions.

1.1. Problem statement

Numerous structural design methods exist for computing member forces in tunnel linings. An exhaustive assessment of these methods, including their advantages and disadvantages, has been conducted by reputable organizations such as The British Tunnelling Society, The Institution of Civil Engineers, and the International Tunnelling Association.

However, when addressing the specific design of cross-passage openings within tunnels, engineers commonly turn to 3D shell-spring models and 3D finite element models. These approaches offer the capability to account for the intricate details of tunnel structures. The 3D finite element method, for instance, excels in capturing the complexities of soil behaviour, encompassing phenomena like soil arching, soil stress history, anisotropy, and variations in soil stiffness and earth pressures due to seepage-induced consolidation around the tunnel.

Nevertheless, the adoption of this method has presented challenges in dealing with joint effects, making the coupling of two rings either infeasible or highly time-consuming for most calculation programs. Additionally, it proves relatively challenging to assess the structural performance of temporary steel supports, which are installed to compensate for reduced tunnel support caused by creating openings in the segmental lining.

Conversely, the 3D shell-spring approach offers the ability to consider critical structural elements within tunnels, including joints and temporary steel support systems. However, it falls short in capturing the complexities of soil behaviour as comprehensively as the 3D finite difference or element approach. Furthermore, the impact of longitudinal and circumferential joints in the shell-spring model, compared to a geotechnical numerical model, has not been thoroughly investigated.

Given the intricate nature of cross-passage junction design, involving nonlinear soil-structure interaction and nonlinear interactions between structural elements, it remains challenging to definitively determine the most suitable method for such applications.

Hence, the primary objective of this study is to conduct an in-depth analysis of the effectiveness of employing 3D finite difference analysis and 3D shell-spring analysis to assess the stress redistribution that occurs due to the creation of cross-passage openings in segmental linings having full structural. To achieve this goal, 3D finite difference and 3D shell-spring models were developed based on a case study, the details of which cannot be explicitly disclosed due to confidentiality constraints.

2. Background and literature review

This chapter will present the background to this thesis in four parts: (1) an overview of ground structure interaction and segmental lining; (2) an overview of cross-passage ground-structure interaction; (3) an overview of the structural design models for tunnels; (4) an overview of numerical modelling in tunnelling.

2.1. Ground-Structure Interaction and Tunnel Lining Load Prediction

Whether employing 2D or 3D numerical modelling, or even analytical solutions, the interaction between tunnels and the surrounding ground is primarily influenced by four key factors. These factors include the stiffness ratio between the ground and tunnel lining, the pre-convergence of the ground, the interface connecting the lining and the ground, and the coefficient of earth pressure at rest. While the last factor is relatively straightforward to grasp, effectively capturing the first three necessitates a deep understanding of tunnel components, the tunnel construction process, and how various modelling methods influence ground-structure interaction and load development. This section will delve into these distinct modelling approaches, with a particular emphasis on segmentally lined tunnels constructed using Earth Pressure Balance Tunnel Boring Machines (EPB TBMs).

2.1.1. Ground Pre-Convergence

Modelling the interaction between the ground and structures through 2D plane strain analysis, whether achieved via numerical modelling or analytical calculations, involves making certain assumptions to simulate the impacts of the 3D tunnelling process. One widely adopted approach for this purpose is the convergence confinement method (CCM). The CCM treats the intricate 3D tunnel excavation and support problem as a simplified 2D problem of ground-structure interaction (AFTES 2001).

The CCM encompasses three primary components (as depicted in Figure 2.1):

1. Ground Reaction Curve (GRC): This curve links the internal pressure (Pi) within the ground to the radial displacement of the tunnel, often referred to as convergence.
2. Support Reaction Curve (SRC): The SRC establishes the relationship between the radial displacement of the tunnel and the support pressure.
3. Longitudinal Displacement Profile (LDP): The LDP connects the tunnel boundary displacement (u) to the tunnel face position (X) and the installation of support. Its primary function is to correlate the support installation point with tunnel convergence (using the GRC) and subsequently with support pressure (using the SRC).

Typically, a normalized displacement ($u* = u/umax$) is expressed as a function of the normalized distance ($X* = X/R0$), where $umax$ represents the maximum tunnel radial displacement at locations where $X* \gg R0$, and $R0$ represents the tunnel radius. Various LDP relationships have been proposed by different researchers, particularly for deep, circular tunnels situated within non-gravitational isotropic stress fields and homogeneous isotropic ground. Panet and Guenot (1982), followed by Panet (1993), developed the initial LDP equations for the linear elastic case behind the tunnel face, which were subsequently refined by Panet (1995):

$$u^*(X) = \frac{u}{u_{max}} = 0.25 + 0.75\left(1 - \left(\frac{0.75}{0.75+X^*}\right)^2\right) \qquad \text{for } X > 0 \qquad (2.1)$$

This solution is not contingent on soil properties. The maximum radial displacement ($umax$) can be ascertained through analytical solutions or 2D numerical computations tailored to the specific scenario under examination. Carranza-Torres and Fairhurst (2000) introduced a comprehensive LDP solution (Eq. 2.2) that encompasses both the region ahead of and behind the tunnel face.

$$u^*(X) = \frac{u}{u_{max}} = \left(1 + e^{\left(1-\frac{2X/D}{1.1}\right)^{-1.7}}\right) \qquad (2.2)$$

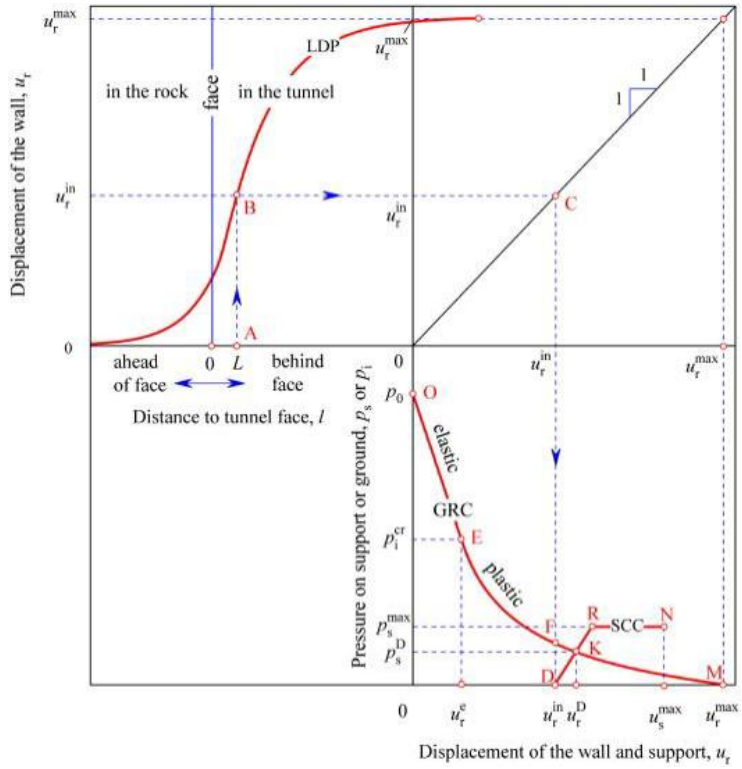

Figure 2-1 Schematic representation of the relation between LDP, GRC, and SCC for use in the Convergence Confinement Method (after Fairhurstand Carranz-Torres, 2002).

Unlu and Gercek (2003) proposed that the LDP does not adhere to a single continuous function but rather comprises two distinct functions: one delineating the LDP ahead of the face (Eq. 2.3) and another characterizing it behind the face (Eq. 2.4).

$$u^*(X) = \frac{u}{u_{max}} = U_0 + A_a\left(1 + e^{\left(-B_a\frac{2X}{D}\right)}\right) \qquad for\ X < 0 \qquad (2.3)$$

$$u^*(X) = \frac{u}{u_{max}} = U_0 + A_b\left(1 + \left(\frac{B_b}{B_b + \frac{2X}{D}}\right)^2\right) \qquad for\ X > 0 \qquad (2.4)$$

Where $U_0 = 0.22v + 0.19,\ A_a = -0.22v - 0.19,\ B_a = 0.73v + 0.81,\ A_b = -0.22v + 0.81$

Vlachopoulos and Diederichs (2009) further refined the LDP relation to accommodate the impact of significant plastic zone development, under the assumption of perfectly plastic conditions without dilation. Their solution remains applicable across a spectrum, ranging from the elastic case to an extended plastic zone scenario. The LDP solution presented by Vlachopoulos and Diederichs (2009) also encompasses both the region ahead of the face and behind the face, employing two distinct equations:

$$u^*(X) = \frac{u}{u_{max}} = u_0^* \cdot e^{(X^*)} \qquad for\ X < 0 \qquad (2.5)$$

$$u^*(X) = \frac{u}{u_{max}} = 1 - (1 - u_0^*)e^{-\frac{sX^*}{2R_p^*}} \qquad for\ X > 0 \qquad (2.6)$$

In this context, R_p^* represents the normalized plastic radius $R_p^* = R_p/R_o$, where R_p is the plastic radius, and u_0^* denotes the normalized radial displacement at the face:

$$u_0^* = \frac{u_0}{u_{max}} = \frac{1}{3}e^{-0.15\left(\frac{Rp}{R_0}\right)} \qquad for\ X = 0 \qquad (2.7)$$

It's worth emphasizing that this solution was initially developed for deep tunnels operating without support, situated in conditions of hydrostatic stress, and within a framework of perfectly elastic-plastic ground. However, many soft grounds tunnelling endeavours involve soil with in-situ stress ratios that deviate from unity and exhibit non-linear soil stiffness. Vlachopoulos and Diederichs (2014) conducted an examination of the limitations associated with the utilization of Equations 2.5 and 2.6 in scenarios characterized by anisotropic stress states and supported tunnels. Their findings revealed that the standard Longitudinal Displacement Profile (LDP) approach (Eq. 2.5 and 2.6) may not provide accurate results under anisotropic stress conditions. Nevertheless, for practical purposes, it can still be employed under the assumption of an isotropic stress state. Vlachopoulos and Diederichs (2014) introduced a revised LDP formula that takes into account the distance from the tunnel face and the position of support installation:

$$u^*(X) = \frac{u}{u_{max}} = \frac{1}{1+e^{0.6\left(1-0.1\frac{S}{R_0}\right)\left(\frac{S}{R_0}-5K_{K_0}-1\right)}} \qquad for\ X > 0 \qquad (2.8)$$

where S is the distance between the face and the support installation position. It is also important to note that no literature was found on the effect pressure balance TBM tunnelling on LDPs, where prior to the installation of the lining, the face of the excavation is supported by muck or slurry pressure, and the shield annulus is assumed to be pressurized as well. However, in common engineering practice, one approach is that u_{max} should be taken as the final radial displacement with an internal pressure according to the machine pressure, while for conventionally excavated tunnels, the LDP is calculated for the unsupported u_{max}.

2.1.2. The behaviour of joints

The stiffness of tunnel support systems plays a crucial role in the interaction between the tunnel structure and the surrounding ground. A stiffer support system has a dual effect: it limits ground deformation but also generates higher loads on the tunnel lining. When dealing with a cast-in-place

concrete ring, the stiffness of the lining ring, which determines its ability to resist deformation, is relatively straightforward to assess.

However, in tunnels supported by pre-cast concrete segmental lining, the impact of joints, particularly longitudinal joints, has been extensively investigated and found to significantly affect the overall behaviour of the lining. Studies conducted by researchers such as Blom (2003), Do et al. (2013a, b), Arnau, and Molins (2011a, b), among others, have highlighted the influence of these joints on the overall stiffness of the lining.

These joints, which are categorized into two types, circumferential (ring) joints between successive rings and longitudinal joints between segments within a single ring, exhibit a lower capacity to resist deformation compared to an intact segment. Consequently, they may reduce the overall stiffness of the tunnel lining. This aspect is illustrated in Figure 2.1, where the significance of these joints in shaping the behaviour of the tunnel lining is evident.

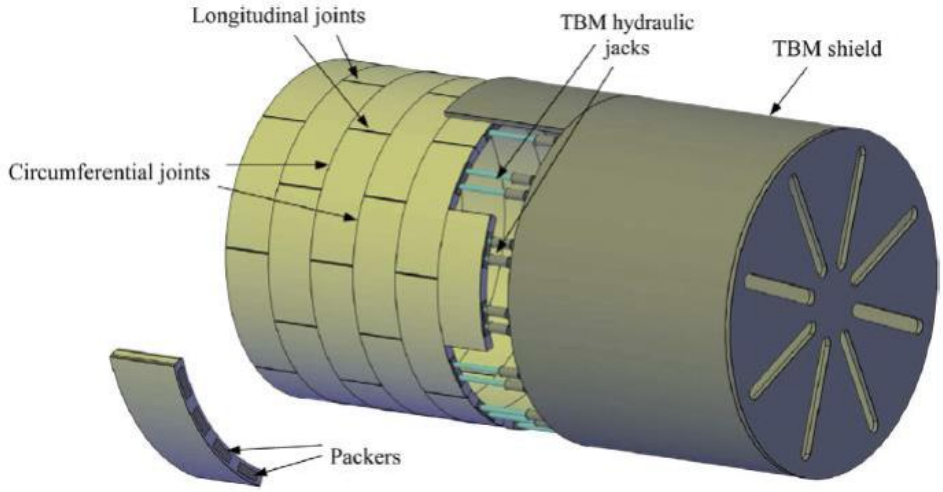

Figure 2-2 Segmental lining and TBM shield. Illustration of circumferential and longitudinal joints within the same ring (Arnau and Molins, 2015).

The influence of joints in tunnel lining analysis is typically addressed through one of two methods: the direct method and the indirect method. In the direct method, each tunnel segment is individually modelled, and connections between segments are established based on specific relationships.

Conversely, the indirect method simplifies the analysis by reducing the rigidity of a continuous tunnel liner model using a reduction factor. This reduction factor, denoted as η, is applied to the bending stiffness (EI) of the continuous tunnel ring, as represented by Equation 2-9.

$$\eta = \frac{EI_{eq}}{EI} \qquad (2.9)$$

One of the earliest approaches to account for the influence of segmental joints and still in widespread use today was developed by Muir Wood in 1975. This method considers the reduction in stiffness based on the number of joints and their geometry. The reduction is achieved by calculating the equivalent moment of inertia using the following approach:

$$I_{eq} = I_j + I_g \left(\frac{4}{n}\right)^2 \left(I_{eq} < I, n > 4\right) \qquad (2.10)$$

Here, I_g and I_j represents the full moment of inertia and the moment of inertia associated with the segmental joint. The calculation of the segmental joint moment of inertia is based on the geometric property defined by the joint neck thickness, which is determined as follows:

$$I_j = \frac{a^8}{12} \left(I_j \ll I\right) \qquad (2.11)$$

Several full-scale testing programs have been conducted to investigate the behaviour of segmental tunnel lining systems. These studies have contributed valuable insights into the performance of such systems under different loading conditions. However, there is a limited number of publications that specifically address the indirect method for modelling segmental rings.

Among the few studies that have explored this approach, Liu et al. (2017) observed that the behaviour of segmental rings under service loading aligns with that of a continuous ring, provided a stiffness reduction factor is back-calculated. However, this research did not delve into the determination of the stiffness reduction factor or the methodologies for its calculation.

In experimental testing publications, the direct rotational stiffness of joints is a commonly discussed topic. Luttikholt (2007), for instance, found that the Janssen (1983) model most accurately represents the moment-rotation behaviour of joints. This model considers the normal force at the joint, which can be either longitudinal or circumferential, and its significant influence on joint behaviour.

When subjected to high normal forces (longitudinal force at circumferential joints or hoop force at longitudinal joints) and low moments, the joint remains closed, exerting only compression pressure on the entire cross-section. However, as bending moments increase, a gap may form when the pressure at the extrados/intrados reaches zero, resulting in significant additional joint rotation. The Janssen model, based on Leonhardt and Reimann (1966), provides a description of joint behaviour in the form of a moment-rotation relationship. Initially, when the joint remains closed and experiences only compression pressure on the cross-section, joint rotation follows a linear-elastic pattern. However, as moments increase and joints begin to open, the rotational stiffness becomes nonlinear.

This understanding of joint behaviour is crucial for accurately modelling segmental tunnel lining systems and ensuring their structural integrity under various loading conditions.

$$\left\{\phi = \frac{Mh}{EI} = 12\frac{M}{Ea^2b}\right\} \; linear\ portion\ M < \frac{1}{6}Na \qquad (2.12)$$

$$\left\{\phi = \frac{8N}{9baE\left(1-\left(\frac{2M}{N-a}\right)^2\right)}\right\} \; non\text{-}linear\ portion\ M > \frac{1}{6}Na \qquad (2.13)$$

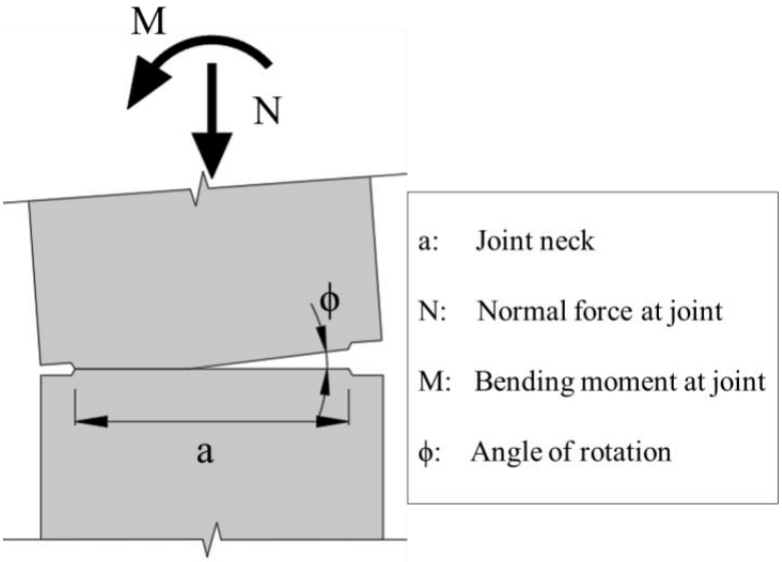

Figure 2-3 Segmental lining concrete hinge (Leonhardt and Reimann).

2.1.3. Ground/Grout Liner Interface

In tunnel engineering, establishing a ground-liner interface is a crucial aspect of the design and analysis process. In the case of shield tunnels with segmental lining, a specific configuration is encountered. Cement grout is injected behind the shield, filling the annular gap between the pre-cast concrete lining and the ground. This means that the pre-cast concrete lining is not in direct contact with the native ground, and the interface between them is different from the interface between sprayed concrete (shotcrete) and the excavation surface.

For analytical solutions, typically two extreme interface conditions are considered. The first is the "full-slip" condition, where there is no transfer of tangential stress between the liner and the ground/grout. The second is the "no-slip" condition, allowing for the transfer of shear tangential stress between the liner and the ground/grout. These conditions are essential for simplifying the analysis of ground-liner interaction.

In numerical analyses of ground-structure interaction, a frictional contact model can also be employed to simulate the interface. In this approach, a zero coefficient of friction corresponds to the full-slip condition, where no tangential shear stress is transferred between the lining and the ground. Given the smooth surface of pre-cast lining segments, it is reasonable to assume that the shear failure criterion between the lining and the annulus grout is closer to full-slip, with low friction and zero cohesion.

The interface model serves as a deformable link connecting the ground/grout medium and the structural element, which is the pre-cast concrete lining. This link is typically described using an elastic or elastic-perfectly plastic relation with a failure criterion, often employing the Coulomb shear strength criterion. A general guideline is to set both the normal stiffness and the tangential stiffness of this interface to be approximately one hundred times the equivalent stiffness of the neighbouring soil element.

The choice between the full-slip and no-slip assumptions significantly impacts the structural response of the tunnel lining. The full-slip assumption results in higher magnitude moments compared to the no-slip assumption and leads to an approximately uniformly distributed thrust force diagram around the tunnel liner. Conversely, the no-slip assumption results in a thrust force diagram that is not uniformly distributed, with the minimum and maximum thrust values depending on the orientation and magnitude of in-situ stress. These considerations are critical for accurately predicting the behaviour of tunnel linings in different ground conditions.

2.2. Cross-Passage Construction

While the construction of cross-passages presents intricate challenges and involves complex 3D interactions between the ground and structures, there is a notable scarcity of research in the literature dedicated to cross-passage openings. The existing body of work can be categorized into two main groups: studies focused on openings within circular tunnels featuring monolithic linings (such as shotcrete or cast-in-place concrete) and investigations cantered around circular tunnels equipped with segmental linings.

2.2.1. Openings in Circular Tunnels

Monolithic Lining

The limited research available on cross-passage construction primarily delves into stress concentration around openings within circular tunnels featuring monolithic linings. This body of work includes studies by Jones (2007), Spyridis and Bergmeister (2015), Battista et al. (2015), and Li et al. (2016). Some of these studies employ elastic closed-form solutions like the Kirsch method to predict stress redistribution within tunnel linings (Jones, 2007 and Spyridis and Bergmeister, 2015).

However, it's important to note that stress redistribution in openings is significantly influenced by ground-structure interaction, as well as the ground-liner stiffness ratio (Spyridis and Bergmeister, 2015).

Jones (2007) conducted an investigation on the stresses within sprayed concrete tunnel intersections using 3D computational modelling and pressure cell measurements from the Heathrow Terminal 5 tunnel. This 3D model included a monolithic shotcrete liner represented by linear-elastic shell elements, connected to a Mohr-Coulomb soil medium. Notably, Jones found that at a distance of 1 meter from the opening, the maximum axial stress concentration factor was approximately two, while the maximum bending stress concentration factor was about 1.5 for the base case model. These findings closely aligned with the pressure cell data obtained from the Heathrow Terminal 5 tunnel. Jones (2007) concluded that stress concentration at tunnel junctions was governed by the construction sequence and the explicit modelling of ground-structure interaction.

Spyridis and Bergmeister (2015) focused their research on ground-structure interaction in circular cross-sections of both parent and child tunnels, considering elastic ground behaviour. The study primarily employed 3D numerical modelling and examined the influence of geometry and the elastic characteristics of the soil, primarily Young's modulus. The ratio of the child tunnel's diameter to the parent tunnel's diameter was varied as 0.6, 0.75, or 0.9, while the ground stiffness ranged from 25 to 100 MPa. The 3D models were calculated in three phases: (1) under geostatic conditions, (2) during the excavation of the parent tunnel and the installation of the lining (without pre-convergence), and (3) after the removal of the breakout (without soil excavation). The results highlighted the substantial impact of soil stiffness and diameter ratio on axial forces and bending moments, with soil stiffness exerting a more pronounced influence. Specifically, reducing soil stiffness led to increased axial force and bending moment, while an increase in the diameter ratio also amplified these effects.

Segmental Lining

The ground-structure interaction involved in cross-passage openings within segmentally lined tunnels is notably more intricate compared to the monolithic case. This complexity arises because one or more rings in the segmental lining are typically severed, disrupting the action of compression hoop forces (see Figure 1.4) and compromising the stability of the ring, as pointed out by Lee and Choi (2017). To address this challenge, various temporary support elements are commonly employed. Among these, the most prevalent include the full ring beam, often humorously referred to as the 'hamster cage,' vertical steel propping, with or without a header beam, and steel segments.

Given the limited body of research available on cross-passage openings in segmentally lined tunnels, designers tend to adopt a highly conservative approach when dealing with cross-passages. This results

in the use of robust but costly temporary support elements. In recent years, coupling elements such as steel dowels and shear bicone dowels have gained popularity (Lee and Choi, 2017, Walter et al. 2019, Ring 2019), offering the potential for reduced construction costs and complexities. However, it's important to note that the utilization of these coupling elements represents a less conservative design approach. The dearth of literature and comprehensive understanding of cross-passage construction and ground-structure interaction may introduce an increased risk of failure in scenarios involving unexpectedly high loads.

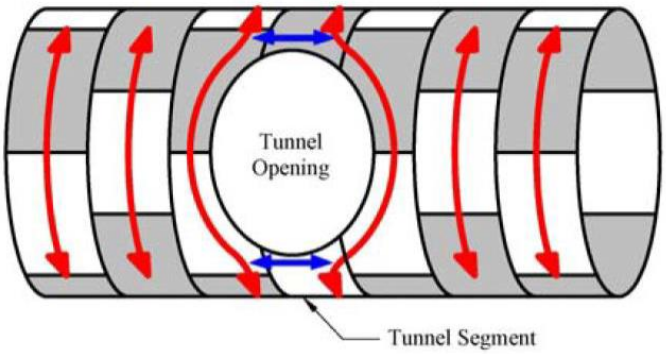

Figure 2-4Stress distribution around opening in segmental tunnel lining (Lee and Choi, 2017), a

Kuyt et al. (2016) conducted a study based on field data collected during the construction of cross-passages between twin segmentally lined tunnels in mixed ground conditions, focusing on data obtained from the Brisbane Airport Link project. In this particular case, the support for the cross-passage openings involved the use of steel segments and hydraulic steel props (refer to Figure 2.5). Vibrating wire strain gauges were strategically placed on the steel segments within the opening, the steel props, and embedded within specific reinforced concrete segments in the vicinity of the opening.

The study identified a significant ground-structure interaction phenomenon: the horizontal unloading effect on the running tunnel lining as excavation progressed toward the breakout. As the excavation advanced toward the breakthrough point, there was a redistribution of stresses ahead of the cross-passage face, leading to changes in the load distribution within the tunnel lining surrounding the breakout area. However, Kuyt et al. (2016) observed that approximately 10% of the loads were transferred onto the segments surrounding the opening. This relatively minor load transfer was attributed to the ground conditions and the presence of installed steel jacking props, which absorbed the majority of the hoop forces generated by the opening ring.

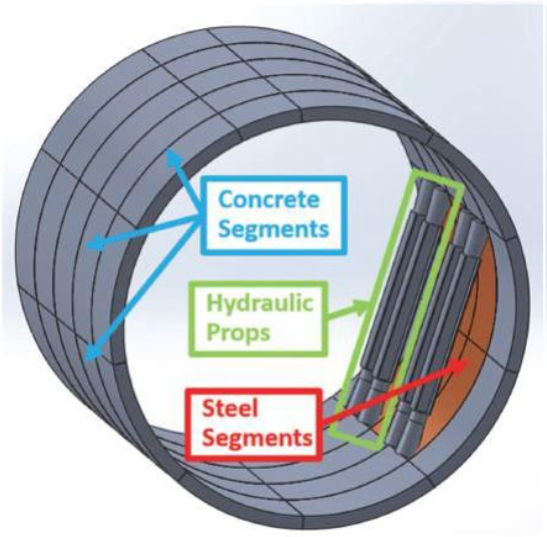

Figure 2-5. cross-passage monitoring components, including strain gauges in the concrete segments, hydraulic props, and steel segments.

Shear bicone dowels have gained popularity in recent years as a means to transfer hoop forces from opened rings to adjacent fully enclosed rings (see Figure 2.6). Depending on the inherent strength of the pre-cast concrete segment, these bicones can offer an allowable shear resistance ranging from 150 to 375 kN per unit run of the ring (as noted by Lee and Choi, 2017). While the shear dowels themselves typically possess sufficient capacity, challenges arise when used in conjunction with thin pre-cast segments, often measuring between 20-40 cm in thickness. This combination presents a challenge due to the risk of concrete failure in shear.

Gehwolf et al. (2016) conducted experimental tests involving four different reinforcement layouts and discovered that the ultimate load capacity of the shear bicone system can vary by as much as 85% based on the specific reinforcement detailing employed. The coupling effect of the temporary support element for the opening plays a crucial role in influencing the structural stiffness, which subsequently impacts the soil-structure stiffness ratio and, consequently, load development. Assessing this coupling effect typically involves 3D ground-structure interaction analysis, a practice commonly carried out in design but seldom documented in the literature.

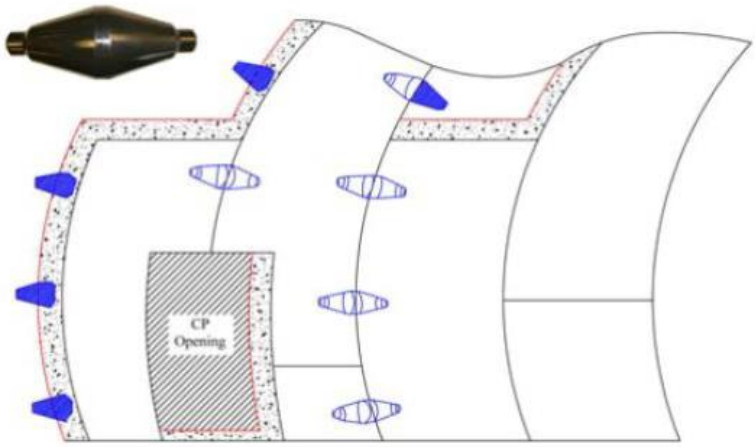

Figure 2-6Illustration of shear bicones in circumferential joint (Lee and Choi, 2017).

2.3. Structural design models for tunnels

Engineers designing tunnels make a commitment to ensure the structural integrity and longevity of tunnel linings. To fulfil this commitment, models reflecting real-world conditions are essential for predicting tunnel behaviour during excavation and throughout its lifespan. The international tunnel construction community employs various analysis methods. Responses to a questionnaire by the ITA working group on Structural Design Models for Tunnelling (1982) reveal notable differences in design approaches among countries, both qualitatively and quantitatively. National-level design methods and recommendations have been developed, incorporating structural design models encompassing analytical closed-form solutions and bedded beam approaches for use in conventional and shield tunnelling.

Different installation procedures for these tunnelling methods significantly affect the magnitude and distribution of loads on tunnel linings. It has been debated in the literature whether it is appropriate to incorporate reduced primary stresses as ground loads. Closed-form solutions of continuum models are often constrained by simplifications, such as assuming circular cross-sections or homogeneous ground. Two-dimensional models based on such simplifications have been widely employed, including in Austria and Germany (ITA, 1982). The bedded beam approach is commonly utilized in German-speaking countries, with some usage observed in Belgium, France, Japan, and the United States (ITA, 1982). These quasi-numerical approaches have advanced to address more complex factors, including non-circular cross-sections or layered ground.

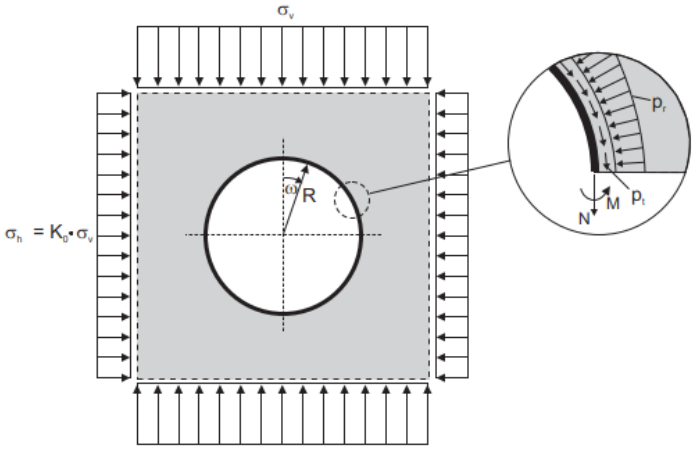

Figure 2-7Continuum model with stresses at infinity

Excavating a tunnel alters the primary stress field, transitioning it from three-dimensional patterns at the tunnelling face to essentially two-dimensional systems farther from the face. Consequently, conventional structural design models focus on two-dimensional stress-strain fields. Although three-dimensional approaches have been proposed by researchers like LOMBARDI (1971) and ERDMANN (1983), they are not widely adopted in engineering practice. Instead, three-dimensional models are typically analysed using numerical finite element or finite difference computations. While elementary models remain prevalent due to their ease of application and qualitative insights, advances in computer capabilities have led to the increasing adoption of finite element approaches.

2.3.1. Analytical solutions of continuum models for lining forces

Ground pressures exerted on tunnel linings are significantly influenced by construction procedures, often leading to extreme pressures during construction rather than afterward. Observations from shield tunnels, such as those reported by CRAIG and MUIR WOOD (1978), indicate the possibility of uneven stresses within a single lining segment, with factors of up to four variations. These uneven stresses may arise from joint twisting or the lining's erection process. Consequently, assessing bending moments and normal forces is challenging, and analyses may not yield precise results. This challenge is particularly pronounced in analytical analyses. However, closed-form solutions offer the advantage of providing direct qualitative insights. Therefore, this discussion will focus on analytical solutions derived from continuum models.

Many analytical solutions are based on several simplifications and assumptions, resulting in a continuum model as depicted in Fig. 2.7. In this model:

1. The circular tunnel with a lining radius (R) is assumed to be sufficiently deep that the increase in stress due to gravity can be disregarded. As a result, the weight of the soil is neglected, and an initially uniform stress field is assumed, with σh representing horizontal stress, σv representing vertical stress, and K0 denoting the coefficient of lateral earth pressure.
2. The lining can be either rough, where both radial (pr) and tangential (pt) stresses are transferred to the lining, or smooth, with no bonding at all (i.e., no tangential stresses exist between the lining and ground).
3. Both the lining and the surrounding ground are assumed to behave linearly elastic.

	Elb-tunnel	Different tunnel linings		
$d\,[cm]$	24	20	25	30
$R\,[m]$	5.30	3.00	4.00	5.00
$A\,[\frac{cm^2}{m}]$	286	2000	2500	3000
$I\,[\frac{cm^4}{m}]$	24418	66670	130210	225000
$\frac{\alpha}{\beta}$	$3.29 \cdot 10^3$	$2.70 \cdot 10^3$	$3.07 \cdot 10^3$	$3.33 \cdot 10^3$

Table 2-1Characteristics of tunnel linings (ERDMANN, 1983)

Analytical solutions for continuum models have a rich history, with SCHMID (1926) likely being one of the earliest contributors. Subsequently, several researchers have presented analytical solutions for bending moments and normal forces in tunnel linings, including BULL (1944), ENGELBRETH (1961), SCHULZE and DUDDECK (1964b), WINDELS (1967), MORGAN (1971), PECK et al. (1972), MUIR WOOD (1975), CURTIS (1975), EINSTEIN and SCHWARZ (1979), and AHRENS et al. (1982). These analytical solutions often utilize relative stiffness parameters to characterize the interaction between the lining and the surrounding ground as

$$\alpha = \frac{ER^3}{E_l I_l} \qquad (2.14)$$

And

$$\beta = \frac{ER}{E_l A_l} \qquad (2.15)$$

$E_l A_l$and $E_l I_l$, respectively represent the normal stiffness and flexural rigidity of the lining. Additionally, E signifies the elasticity modulus of the adjacent ground. ERDMANN (1983) further

expanded upon the research by AHRENS et al. (1982) to provide simplified solutions for computing normal forces (N) and bending moments (M) in tunnel linings.

$$N = N_0 + N_2 \qquad \text{and} \qquad M = M_2$$

$$N_0 = \frac{\sigma_v + \sigma_h}{2} \cdot R \cdot n_0 \qquad (2.16)$$

$$\begin{bmatrix} N_2 \\ M_2 \end{bmatrix} = \frac{\sigma_v - \sigma_h}{2} \cdot \begin{bmatrix} R \cdot n_2 \\ R^2 \cdot m_2 \end{bmatrix} \cdot cos\ 2\omega \qquad (2.17)$$

In the context of the formulas presented, the subscript "0" signifies a constant load, while the subscript "2" denotes a varying load dependent on the angle ω, as illustrated in Figure 2.7. The coefficients n_0, n_2 and m_2, which pertain to bending moments and normal forces, can be observed in Figures 2.8 to 2.10. These figures provide data for full bonding, tangential slip, and various Poisson's ratios (ν) of the surrounding ground.

The coefficients n_0, n_2 and m_2, as depicted in Figures 3.14 to 3.16, are derived for a relative stiffness ratio of $\alpha/\beta = 3 \cdot 10^3$. Notably, these coefficients increase as the relative stiffnesses α and β decrease. While tunnels with a radius of 5 meters typically exhibit α/β ratios ranging from 1000 to 5000, such variations have minimal impact on the curves shown in Figures 2.8 to 2.10 (ERDMANN, 1983). Table 3.2 provides typical ratios for tunnel linings.

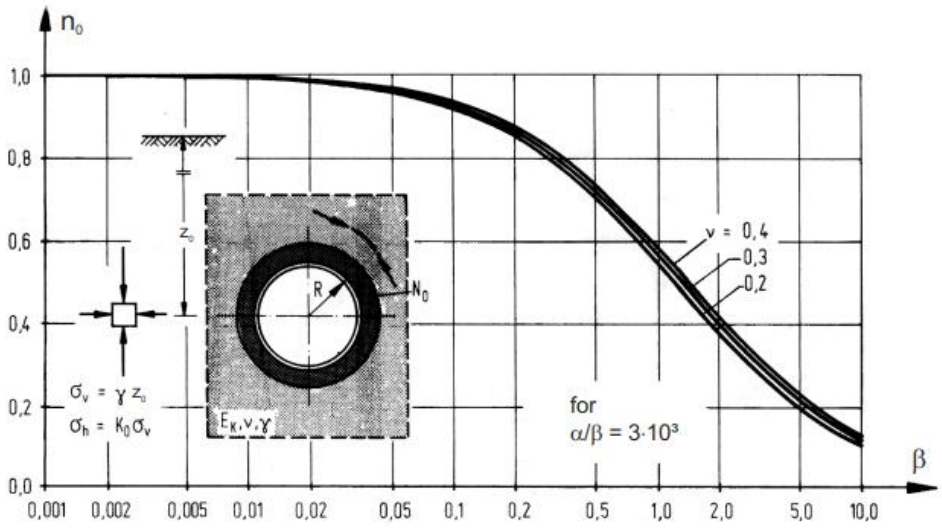

Figure 2-8 Coefficient n_0 for constant part of normal force (ERDMANN, 1983)

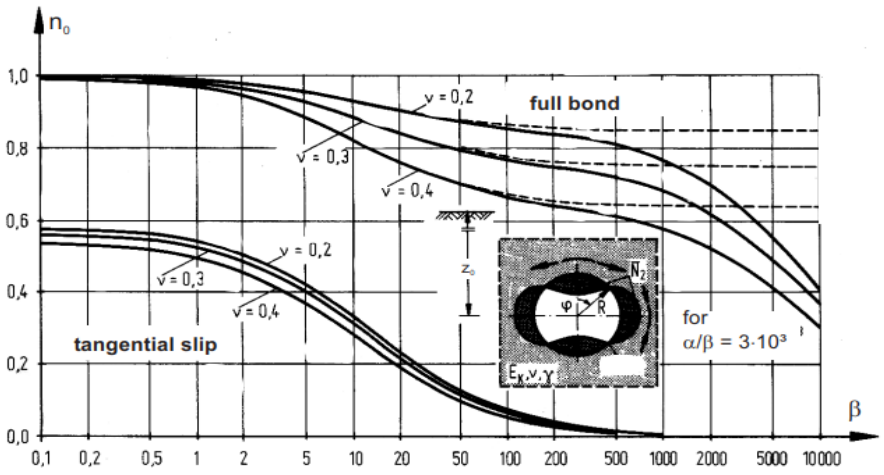

Figure 2-9 . Coefficient n_2 for non-constant part of normal force (ERDMANN, 1983)

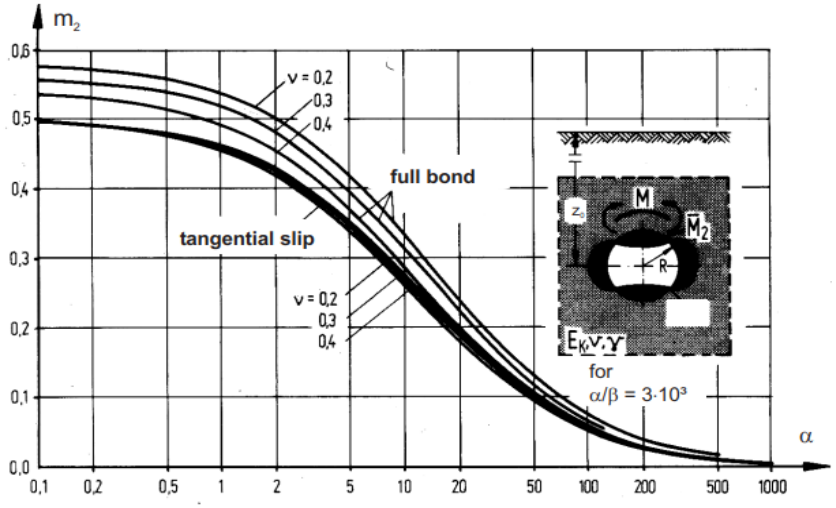

Figure 2-10 Coefficient m_2 for bending moment (ERDMANN, 1983)

Bending moments exhibit a linear dependence on the deviatoric stress (σv − σh)/2, which is influenced by tunnel depth and installation methods. To incorporate installation procedures, the stress reduction method can be directly applied to the stresses described in Eqs. 2.16 - 2.17 of the analytical solution. Alternatively, tunnel installation can be considered using a displacement approach, as demonstrated by CHOU and BOBET (2002). They conducted a study involving 28 shield tunnels, identifying gap values between the lining and ground ranging from 10mm to 288mm, depending on tunnel radius and installation procedures. While information on the "gap" could potentially be converted into a stress reduction and applied to analytical solutions, this approach may be cumbersome. Instead, analytical solutions can be more seamlessly integrated with the stress reduction method.

2.3.2. The bedded-beam model

The continuum approach described above may be suitable for very deep tunnels in uniform ground but is not well-suited for shallow tunnels in layered ground or non-circular tunnels. To address these limitations, the bedded-ring model was developed. In this model, springs replace the ground reaction, and external forces are applied to represent lining loads. While this approach allows for the calculation of structural forces and lining deformations, it does not provide information on settlements.

It's important to note that this brief overview of contributions to the development of bedded beam approaches is not exhaustive, as several significant contributions have been omitted. BULL (1944) is credited as one of the earliest proponents of the bedded beam approach.

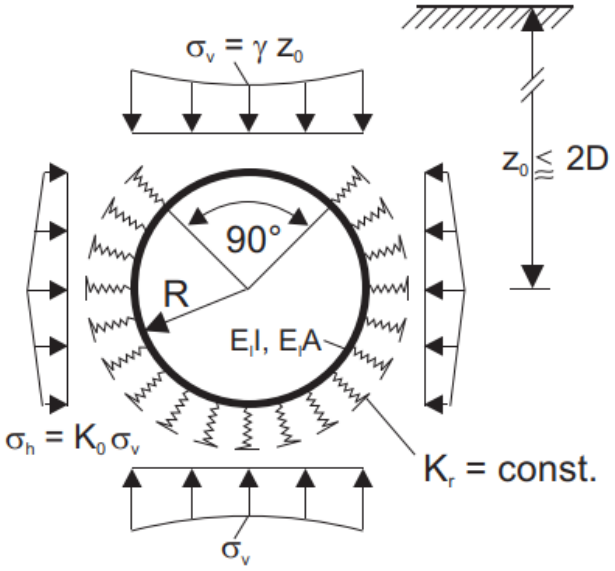

Figure 2-11. Example of a bedded-beam model for shallow shield tunnels in soils (DUDDECK and ERDMANN,1982)

Erdmann's approach involves dividing the tunnel ring into 16 equal divisions, with the external ground loads combined to create 16 point loads, each acting on one of these divisions. The ground reaction forces are determined by spring constants. Other significant contributions to this approach were made by ROZSA (1963), SATTLER (1965), WINKLER (1970), and WAGNER et al. (1980).

Models that are still utilized in contemporary engineering practice were introduced by DUDDECK (1972). He distinguishes between shallow tunnels with z0 < 2D (where D represents the tunnel diameter) and deep tunnels with z0 ≥ 3D. For shallow tunnels, a model is proposed as shown in Fig. 2.11. In this model, bedding is considered only in regions where lining deflection pushes outward, resulting in ground compression. At the tunnel crown, where the lining deforms inward, no tension

bedding is applied. Typically, a non-bedded lining arc length with an angle of 90° - 120° is assumed. Simultaneously, a ground load with the magnitude of the full vertical overburden is assumed to act on the non-bedded tunnel crown.

According to the ITA (1988) working group on General Approaches to the Design of Tunnels, a design model like the one shown in Fig. 2.11. be well-suited for designing linings for shallow shield-driven tunnels in soil. For deep tunnels, a bedded beam model as presented in Fig. 2.12 may be applied. Using support mechanisms such as anchors, the ground is actively involved in the tunnel structure to carry a significant portion of the load. An idealized ground-lining ring, as shown in Fig. 3.18, is proposed. The thickness of the incorporated ground ring depends on the active anchor length. This ring doesn't need to be circular, and non-circular cross-sections like a horseshoe profile can also be considered.

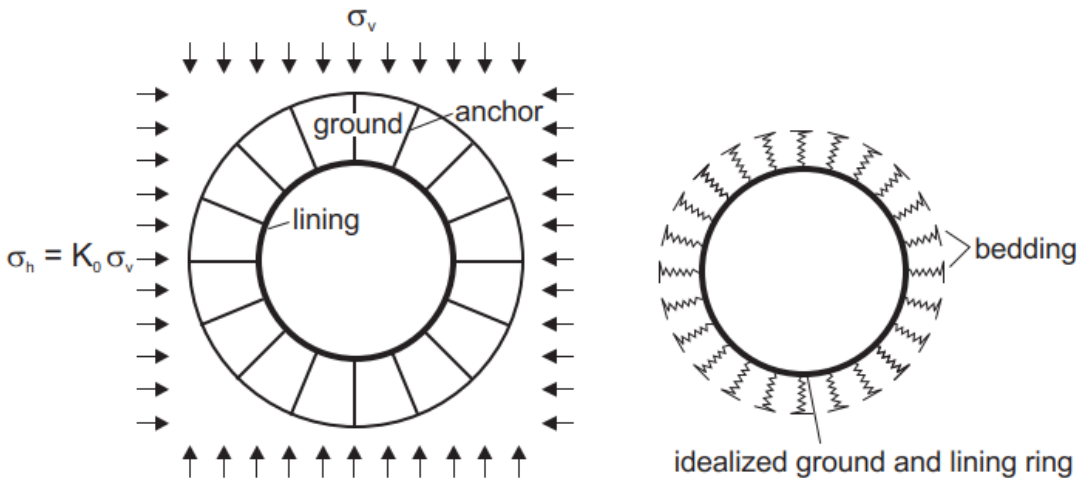

Figure 2-12: Example of a bedded-beam model for deep tunnels (DUDDECK, 1979)

2.3.2.1. Spring constants for bedding

Bedded beam approaches are based on the ground behaviour hypothesis introduced by WINKLER (1867), which describes the relationship between load and deformation as follows:

$$p = k\phi S \qquad (2.18)$$

given p as the ground bedding pressure, S as the radial displacement of the tunnel and k as the ground reaction modulus. In numerical bedded beam approaches, the ground bedding is represented by a series of discrete springs positioned at regularly spaced intervals along the tunnel lining. These springs serve to model the interaction between the ground and the tunnel structure. Each spring is associated with a specific spring stiffness denoted as K_{spring} . This approach allows for a pointwise

consideration of ground behaviour, meaning that it doesn't incorporate interactions with neighbouring regions. Instead, it focuses on the localized behaviour of the ground at specific locations along the tunnel's perimeter.

$$K_{spring} = a\phi b\phi k \qquad (2.19)$$

given a and b as the distance of springs in the transverse and longitudinal cross-section respectively.

To incorporate radial bedding into a numerical bedded beam calculation, it's necessary to determine a radial ground reaction modulus, which is denoted as $\mathbf{k}_r$. Additionally, tangential shear bedding can be modelled using a separate ground reaction modulus called $\mathbf{k}_t$, with tangentially placed springs. For a circular tunnel in elastic ground subjected to axisymmetric loading, the ground reaction (bedding) is primarily dependent on the tunnel's radius and the ground's elasticity parameters. In such cases, the analytical solution for the radial ground reaction modulus can be calculated using specific formulas.

$$k_r = \frac{1}{1+v}\phi\frac{E}{R} \qquad (2.20)$$

In bedded beam approaches for circular tunnels in elastic ground under axisymmetric loading, the radial ground reaction modulus k_r can be determined based on the Poisson's ratio v and the Young's modulus of the ground E. Using the theory of elasticity, it can be deduced that when the Poisson's ratio v is equal to 1/3, the Young's modulus E is related to the constrained modulus, also known as the oedometer modulus E_{oed}, by the equation: E = 2/3 * E_{oed}. Substituting this relationship into Equation 2.20, you obtain the often used a simplified relation

$$k_r = \alpha.\phi\frac{E_{oed}}{R} \qquad (2.21)$$

Determining the factor α can be a challenging task in engineering practice since the radial ground reaction modulus k_r is not a material constant; it significantly depends on the geometry of the structure. Engineers often resort to in situ tests, like plate loading tests, even though these tests may not perfectly represent the final tunnel geometry. They use these tests to estimate suitable values for α (ITA, 1982).

In German engineering practice, various values for @ ranging from 0.66 to 3.0 have been suggested (MU¨LLER-SALZBURG, 1978). However, it's worth noting that α= 1 is a commonly used value (DUDDECK, 1980). The choice of α depends on project-specific conditions and engineering judgment.

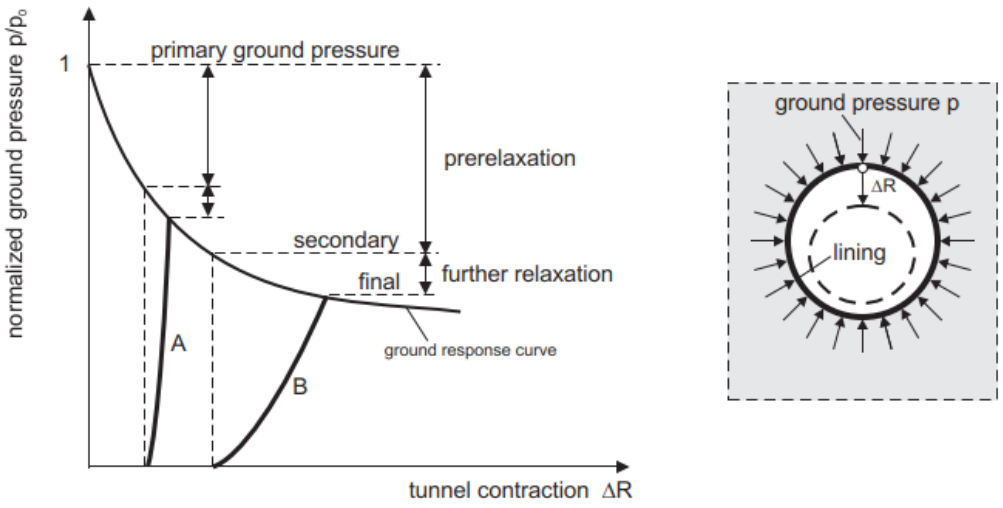

A lining response curve of closed face tunnelling

B lining response curve of open face tunnelling

Figure 2-13 Illustration of development of ground pressures on tunnel linings adopting ground response curve.

2.3.3. The Shell-Spring model

The Shell-Spring Method is a numerical approach utilized to analyse tunnel lining behaviour, particularly in the context of segmental or ring-shaped linings commonly employed in tunnel construction. Fundamentally, this method involves representing the tunnel lining as interconnected shell elements, each possessing distinct mechanical properties. These properties encompass characteristics like thickness, material traits, and the capacity to undergo deformation or rotation at joints. At its core, the Shell-Spring Method excels in capturing the discrete nature of tunnel lining construction by modelling individual segments or rings as distinct shell elements. These elements are further interconnected through spring elements, which replicate the stiffness of joints connecting these segments. This approach allows for the computation of forces, displacements, and deformations at these interfaces, enabling a detailed examination of segmental behaviour and joint performance.

The Shell-Spring Method finds natural application in the analysis of tunnels characterized by segmental or ring-shaped linings. Its versatility and precision render it an invaluable tool for assessing the influence of various factors encountered during tunnel construction and operation. Notable applications encompass:

1. **Segment Installation Analysis:** This method excels in evaluating the stresses and deformations incurred during tunnel segment installation. It takes into account each segment's properties and the interaction at joints, enabling engineers to assess lining structural integrity and safety during this critical phase.

2. **Joint Behaviour Assessment:** Offering an intricate understanding of joint behavior within the tunnel lining, this method aids in discerning how joints accommodate load transfer, deformations, and potential misalignments between adjacent segments.
3. **Cross-Passage Creation:** Valuable in projects involving cross-passage construction within tunnels, the Shell-Spring Method assesses the effect of these openings on lining integrity. It facilitates the study of segmental lining responses to localized changes in geometry and loading.
4. **Construction Activity Impact:** Useful for evaluating the influence of various construction activities, such as grouting, ring closure, or shield jacking, on tunnel lining performance.

Figure 2-14 illustration of one ring lining (SAP2000)

While both the Shell-Spring Method and the Bedded Beam Spring Method serve as structural analysis techniques, they exhibit significant disparities in structural representation and application. These distinctions are pivotal in selecting the most suitable method for a given tunnel engineering scenario.

The Shell-Spring Method characterizes the tunnel lining as interconnected shell elements, representing individual segments or rings, each with specific properties and the capacity to deform or rotate at joints. Conversely, the Bedded Beam Spring Method simplifies the tunnel lining as a continuous beam element supported by a foundation or bed, neglecting the discrete nature of segments and joints for a more continuous model.

The choice between these methods hinges on the specific characteristics of the tunnel lining and the level of detail required for analysis. The Shell-Spring Method is well-suited for projects involving

segmental tunnel linings and intricate jointed systems where granular analysis is imperative. In contrast, the Bedded Beam Spring Method is often applied to tunnels featuring more continuous or monolithic linings, where segmental details and joint behaviour play a less critical role.

The Shell-Spring Method enables in-depth examination of segmental behaviour, joint performance, and localized responses, making it ideal for scenarios where precise interaction between individual segments is paramount. Conversely, the Bedded Beam Spring Method provides a broader perspective on tunnel lining behaviour, suited for expedient, simplified analyses, particularly when segmental characteristics are less significant.

In conclusion, the Shell-Spring Method assumes a pivotal role in tunnel engineering, offering unmatched insights into segmental tunnel linings and their interactions with the surrounding ground. Its capacity to model discrete segments and joints distinguishes it from the Bedded Beam Spring Method, rendering it particularly valuable for projects involving segmental tunnel linings and the detailed analysis of jointed systems.

2.3.4. Ground pressures on tunnel linings

The deformations that occur during tunnel installation procedures lead to a reduction in primary ground pressures and create loads on the tunnel lining. These loads represent a fraction of the primary ground pressures that act on the supporting lining. Several factors influence the distribution and magnitude of ground pressures on tunnel linings, including the stiffness of the ground and lining, tunnel cross-section geometry, and installation methods. To accurately estimate the distribution and magnitude of ground pressures, tunnel design must consider these factors and their interactions.

Figure 2.13 illustrates the development of ground pressures on tunnel linings using the ground response curve. It shows that the amount of ground pressure on the tunnel lining is affected by the reduction in primary ground pressures before the installation of the lining. Tunnel excavation leads to stress pre-relaxation in the ground, reducing primary ground pressures to a secondary state of stress. The extent of stress pre-relaxation depends on the tunnelling method, such as closed-face or open-face tunnelling. Closed-face tunnelling minimizes ground deformations, resulting in relatively small stress pre-relaxation. In contrast, open-face tunnelling, where unsupported cut stretches are excavated, leads to significant ground mobilization and higher stress pre-relaxation.

To ensure ground stability after tunnel excavation, a lining is installed. Lining deformation further relaxes the stress in the surrounding ground, reducing secondary ground pressures to their final values on the tunnel lining. Stiff pre-cast segmental linings, commonly used in shield tunnelling, generally

exhibit smaller lining deformation. In conventional tunnelling, lining deformation may be more substantial. Figure 2.13 demonstrates that the effect of further stress relaxation due to lining deformation is relatively small compared to stress pre-relaxation.

To assess structural forces in tunnel linings using an appropriate structural model, both stress pre-relaxation and further stress relaxation need to be considered. Analytical solutions of continuum models or bedded beam calculations automatically account for lining deformations resulting from ground loading and the associated further stress relaxation of the ground. However, these methods do not automatically account for the effects of stress pre-relaxation, and assumptions about its magnitude must be made.

In addition to stress pre-relaxation, it's crucial to consider the distribution of primary ground pressures in tunnel analysis. Different structural models with various primary ground pressure distributions on the tunnel lining are depicted in Figure 2.15. These distributions are chosen based on factors like tunnel depth, with increasing primary horizontal pressures with depth used for shallow tunnels (Figure 2.15 ‘1’), constant horizontal pressures for deep tunnels (Figure 2.15 ‘2’) and decreasing horizontal stresses with depth (Figure 2.15 ‘3’), although the reason for the latter is not commonly explained in the literature.

Secondary ground pressures

The magnitude of secondary ground pressure is influenced by the cumulative effects of all stress redistributions that occur during tunnel excavation. Prior to the installation of the tunnel lining, stress redistribution occurs in front of the tunnel face and around the shield machine (or around the unsupported cut-stretch in conventional tunnelling), leading to stress pre-relaxation. Depending on tunnel installation procedures, tunnel depth, and ground properties, stress pre-relaxation can be significant, resulting in a substantial reduction in secondary ground pressures.

DUDDECK and ERDMANN (1982) differentiate between shallow tunnels with depths (z0) greater than or equal to 2 times the tunnel diameter (2D), moderately deep tunnels with depths ranging from 2D to 3D, and deep tunnels with depths greater than or equal to 3 times the tunnel diameter (3D). For shallow and moderately deep tunnels, they suggest that no stress pre-relaxation occurs at the crown of the tunnel, and full primary stresses are applied on top of the tunnel, as depicted in Fig. 2.11. Consequently, it is assumed that, in the long term (several years after tunnel construction), the ground will eventually return to a condition nearly identical to its state before tunnelling. Changes in groundwater levels, traffic vibrations, and other factors may trigger this readjustment.

Indeed, CRAIG and MUIR WOOD (1978) report that instrumentation of existing shallow tunnels, which were 50 to 75 years old and had to be dismantled during the construction of new works, showed combined hoop and bending stresses in the lining equivalent to the overburden pressure. For tunnels in sandy soils below the water table, they noted that measurements revealed combined stresses between 80% and 100% of the equivalent overburden stress, which could develop within the first few months.

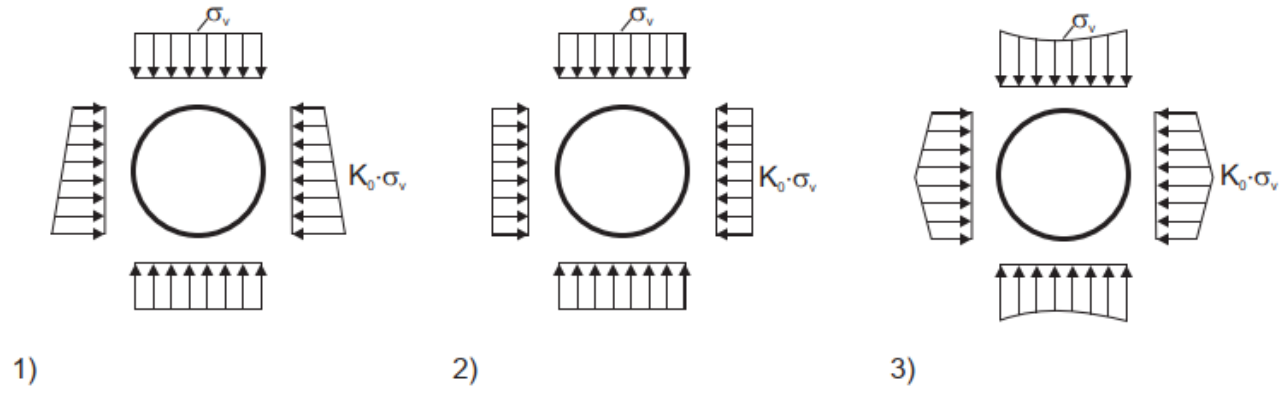

Figure 2-15. Different ground loads distributions of on tunnel linings, ***1)*** *HEWETT and JOHANNESSON (1922),* ***2)*** *WINDELS (1967),* ***3)*** *SCHULZE and DUDDECK (1964a), HARTMANN (1970), FLECK and SKLIVANOS (1978)*

In the case of deep tunnels, it becomes evident that some level of stress pre-relaxation must be considered to reduce the loads on the lining. DUDDECK and ERDMANN (1982) argue that regardless of tunnel depth, allowance should be made for potential variations in ground stresses concerning factors such as cohesion, ground stiffness, tunnel ring closure time, excavation procedure, lining erection method, time-dependent behaviour of the ground and the lining, and the influence of groundwater. Thus, the transition from shallow to deep tunnels is not sharply defined, and the three cases (shallow, moderately deep, and deep tunnels) overlap.

To account for the installation of closed-face tunnelling, MUIR WOOD (1975) proposed considering only 50% of the initial ground stresses. Indeed, in present two-dimensional numerical analyses of open-face tunnelling, a stress reduction factor, often referred to as the unloading or beta factor, of approximately 50% is commonly used. However, this value appears to be relatively low for modern closed-face tunnelling. Because open-face tunnelling typically mobilizes the shear strength of the ground to a relatively high degree, this method requires ground with noticeable cohesion, and consequently, a significant amount of stress pre-relaxation may generally be justified.

The topic of ground pressures on tunnel linings with regard to different structural design models, tunnel depths and ground stiffnesses has also been reviewed by the ITA (1988)-working group on

General Approaches to the Design of Tunnels. Fig. 2.16 categorizes four different approaches of structural design models:

(1) continuum model for deep tunnels, empirical approach for ground pressures.

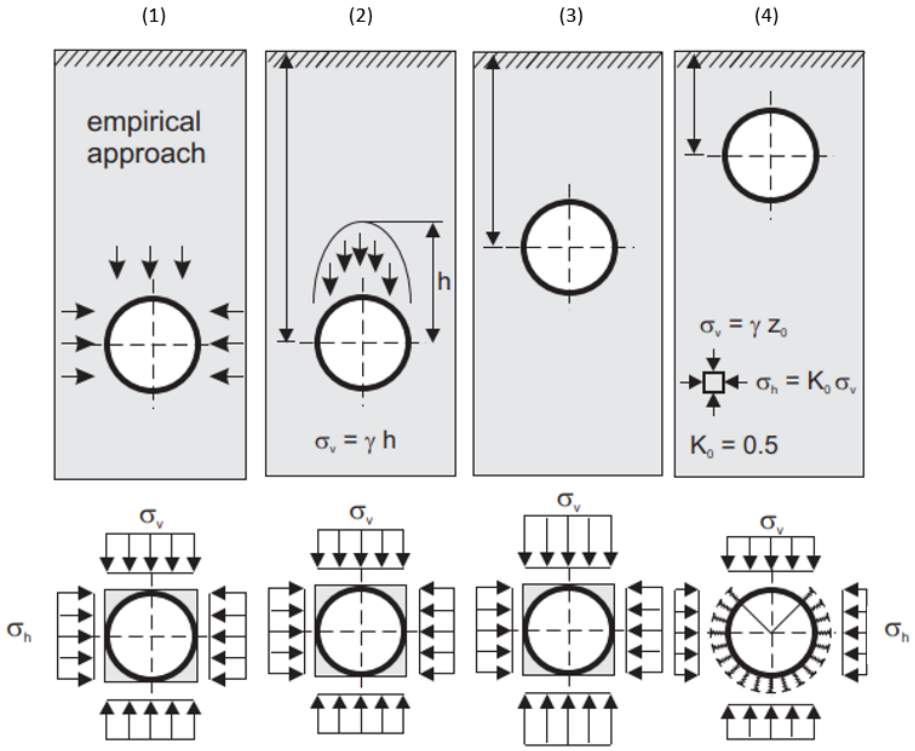

Figure 2-16 Plane-strain design models for different depths and ground stiffnesses (ITA,1988)

(2) continuum model for deep tunnels in stiff ground.

(3) continuum model for tunnels at shallow depth and moderately stiff ground.

(4) bedded-beam model for very shallow tunnels in soft ground.

For tunnels at shallow depths in soil, immediate support must be provided by a relatively stiff lining. Here, it is agreed that the three-dimensional stress release at the face of the tunnel during excavation may be neglected. In case (1), the ground stresses acting on the lining are determined by an empirical approach, which may be based on previous experiences with the same ground and the same tunnelling method, in-situ observations and monitoring of initial tunnel sections, interpretation of observed data, and continuous improvements of the design model. Here, some reduction of stresses may generally be incorporated. Case (2) assumes that some stress pre-relaxation is caused by deformations that occur before the lining participates. In rock or highly cohesive soil, the ground may be strong enough to

allow for a certain unsupported section at the tunnel face. Stress pre-relaxation is also assumed for tunnels with a high overburden, and a reduction of the acting crown pressure (as represented in Fig. 3.21 by $h < z_0$) is taken into account. Confirming these recommendations, CRAIG and MUIR WOOD (1978) discuss measurements of tunnels in rock, where readings have been taken of the stresses in the arch ribs prior to the casting of a cast in-situ lining. Their presented results generally show relatively low stresses. In cases (3) and (4) of Fig. 2.16, no stress pre-relaxation is taken into account, incorporating full primary ground pressures.

2.4. Numerical Modelling in Tunnelling

The historical development of numerical modelling in tunnel engineering mirrors the advancement of computing technology and the increasing complexity of tunnel projects. Originating in the 1960s when early computers became accessible to engineers, this field started with basic numerical methods like the Finite Element Method (FEM) and Finite Difference Method (FDM), providing a foundation for analysing tunnel behaviour and interactions with the surrounding ground. In the 1980s and 1990s, numerical modelling in tunnelling experienced rapid growth, driven by improved computing power. This era witnessed the creation of specialized software packages and advanced algorithms, instrumental in modelling various aspects of tunnelling, including ground support systems, excavation processes, and structural responses. Commercial tunnel design software gained prominence. The 21st century brought further refinements, including three-dimensional modelling and advanced constitutive models for simulating soil and rock behaviour. Integration of Geographic Information Systems (GIS) data enhanced geotechnical analyses, and the Distinct Element Method (DEM) became valuable for simulating blocky ground conditions. Tunnel Boring Machine (TBM) simulation became a hallmark, optimizing excavation procedures and risk assessment. Modern numerical modelling in tunnelling prioritizes sustainability and environmental impact assessment, evaluating factors like groundwater flow, soil settlement, and thermal interactions with surroundings. In summary, the historical evolution of numerical modelling in tunnelling aligns with the increasing complexity of tunnel projects and computational advancements. Today, it is an indispensable tool in tunnel engineering, supporting design, analysis, and safe execution of global tunnelling projects.

2.4.1. The Finite difference method

Among the various numerical techniques, Finite Difference Method (FDM) stands out as one of the oldest methods used to approximate solutions for Partial Differential Equations (PDEs) in the field of engineering. It involves a mathematical expression in the form of $f(x + xa) - f(x + xb)$. When a finite difference is divided by $xb - xa$, it results in a difference quotient. To put it simply, the Finite

Difference Method relies on discretizing a function on a grid (as depicted in Figure 2.17). The approximation of derivatives through finite differences plays a pivotal role in numerical solutions, particularly in addressing boundary value problems.

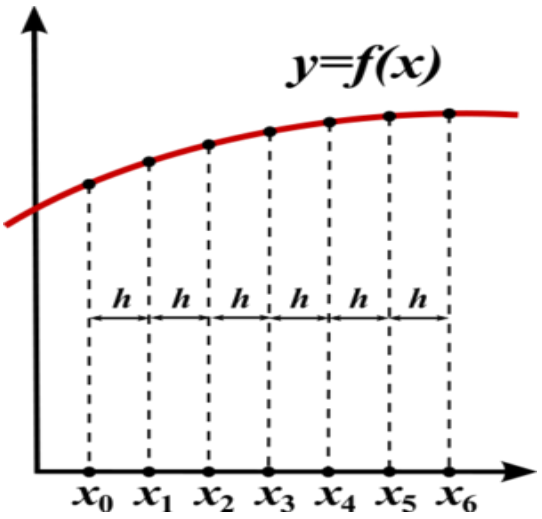

Figure 2-17 discretization of a typical problem domain

FDM is typically founded on a Taylor series representation of a function. The precision of this approach is contingent upon the order of approximation employed. In simpler terms, accuracy is linked to the number of terms utilized in representing the function via the Taylor series. This method finds extensive application in rock engineering, particularly in seismic modelling, where a discretized version of the wave equation can be derived. This discrete model allows the propagation of the wave field, originating from the source location (initial conditions). It's important to note that the accuracy of derivative calculations, for a given order, is influenced by the grid spacing. A smaller grid size yields higher accuracy but demands more time and memory for computations.

In the FDM framework, the typical approach involves replacing the partial derivatives of the target function (e.g., displacement) with differences defined over specific intervals in the coordinate directions, denoted as $\Delta x, \Delta y,$ and Δz. Consequently, a system of algebraic simultaneous equations related to the predefined objective function can be associated with each node within the grid system spanning the domain of interest.

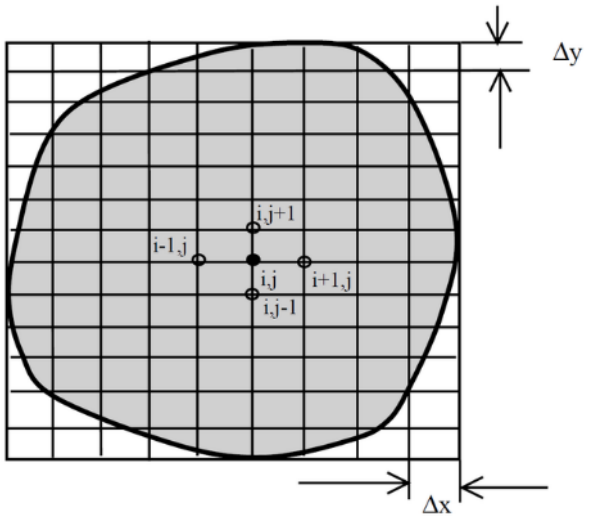

Figure 2-18 illustration of a 2D FD grid

For an elastic solid in 2-D, the FDM equation of equilibrium at a point like $(i,j)$is given as:

$$u_x^{i,j} = a_1 u_x^{i-1,j} + a_2 u_x^{i,j-1} + a_3 u_x^{i,j+1} + a_4 u_x^{i+1,j} + a_5 u_x^{i+1,j+1} + a_6 F_x^{i,j}$$
$$u_y^{i,j} = b_1 u_y^{i-1,j} + b_2 u_y^{i,j-1} + b_3 u_y^{i,j+1} + b_4 u_y^{i+1,j} + b_5 u_y^{i+1,j+1} + b_6 F_y^{i,j}$$

the coefficients ak and bk, representing the elastic properties of the solid, are functions determined by the grid intervals Δx and Δy. On the other hand, Δx and Δy and $F\_x\hat{}(i,j)$ and $F\_y\hat{}(i,j)$ represent the body forces acting at the point(i,j) within the domain. Additionally, it's essential to establish appropriate boundary conditions at the boundary nodes of the domain. These boundary conditions play a crucial role in determining the behaviour of the system. By considering these boundary conditions, solving the simultaneous algebraic system of equations will yield the required values for the objective function at all nodes within the computational domain. These values represent the solution to the problem under consideration.

2.4.2. FLAC3D

developed by the ITASCA consulting group, a powerful numerical command driven (i.e., FISH and python scripting languages) modelling software for advanced geotechnical analysis of materials like soil, rock, or any substance that may exhibit plastic flow behaviour under certain conditions, where materials are represented using elements or zones, forming a grid that can be customized by the user to match the geometry of the object being modelled. It serves as a valuable tool for geotechnical, civil, and mining engineers in various problems that demand continuum analysis for a comprehensive

understanding of complex scenarios and geological formations, offering 26 Mechanical and 9 creep Constitutive models along with the ability to create your own one. FLAC3D follows 3 approaches in solving problems:

The finite volume where first-order space and time derivatives of a variable are approximated by finite volumes assuming linear variations of the variable over finite space and time intervals, respectively.

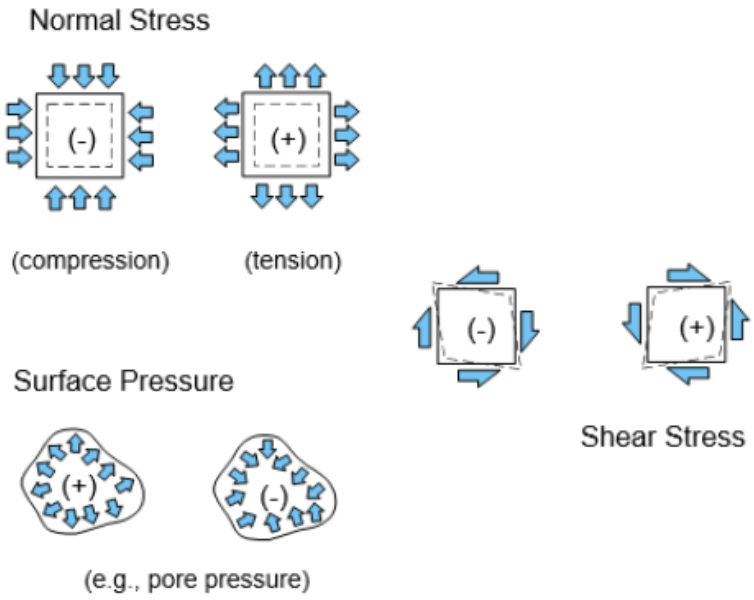

Figure 2-19 Sign convention for stresses in FLAC3D

The discrete model where the continuous medium is replaced by a discrete equivalent one in which all forces involved (applied and interactive) are concentrated at the nodes of a three-dimensional mesh used in the medium representation.

The Dynamic-solution approach where the inertial terms in the equations of motion are used as numerical means to reach the equilibrium state of the system under consideration.

Grid and discretization

Grid or Mesh is an assemblage of one or more finite volume zones across the physical region that is being analysed. These zones are cornered by a number of points known as Gridpoints, depending on the shape the zone has.

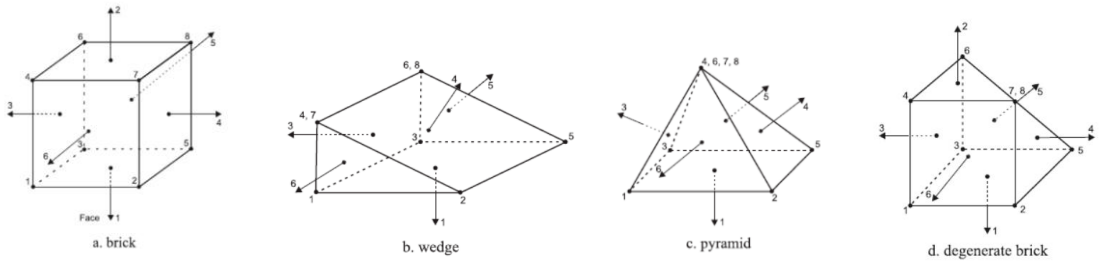

Figure 2-20 typical zone geometries within FLAC3D

Grid discretization in FLAC3D is vital for geotechnical and geomechanical simulations, as It divides the spatial domain into discrete elements, where the size of these grids impacts the accuracy and efficiency of the analysis. FLAC supports several types of grids, regular, irregular, and unstructured grids, chosen based on problem complexity, as smaller grid sizes enhance accuracy for localized phenomena, while larger ones suit broader geological behaviour modelling. Usually, typical problems are characterized by grids comprising hundreds, thousands, or even millions of zones. The grid is described using global x, y, and z coordinates, with gridpoints and zone centroids located through their respective (x, y, z) position vectors. Each gridpoint and zone is uniquely identified by an ID, serving as a reference for that particular element. Grid generation in FLAC3D involves the adjustment and shaping of the mesh to conform to the physical domain's geometry. This process can be executed through various methods, including commands that construct zones from basic shapes, FLAC's interactive extrusion and building blocks features, or by applying advanced mesh generation techniques using external tools.

Figure 2-21 quadrilateral and tetrahedral meshes

Boundary conditions

Boundary conditions in numerical modelling, particularly in FLAC3D, involve specifying field variable values like stress and displacement at the model's boundary. These boundaries are classified into two categories: real and artificial. Real boundaries represent physical features, such as the surface of a tunnel or the ground, while artificial boundaries like symmetry and truncation planes are introduced to enclose a defined number of zones.

Mechanical conditions applied at these boundaries fall into two primary types: prescribed displacement and prescribed stress. For stress boundaries, FLAC3D grids are initially stress-free. Stresses or forces can be applied to any boundary using the “zone face apply” command, specifying the direction in global or local coordinates.

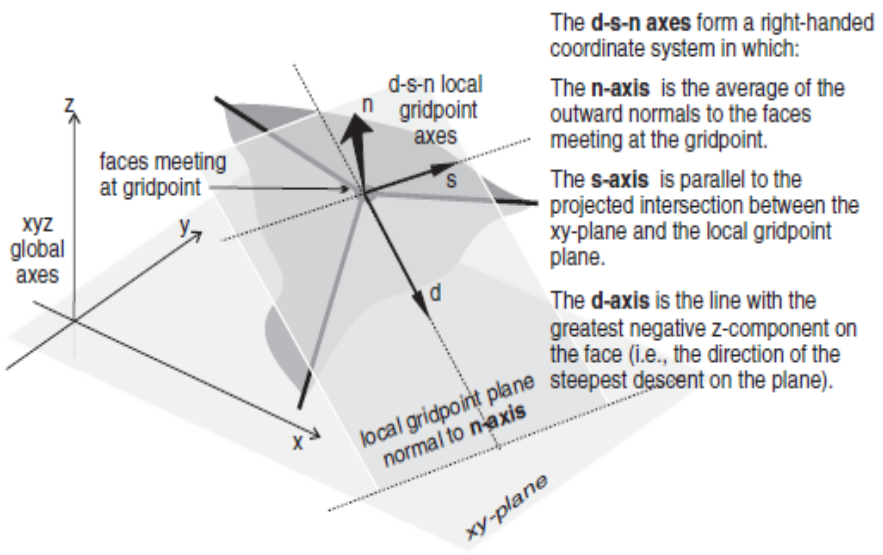

Figure 2-22. Local gridpoint axes defined by (d) dip direction, (s) strike direction, and (n) normal direction.

The range for this command determines which faces are affected, and FLAC3D calculates stresses as tractions resulting from the stress tensor acting on the boundary plane.

In the case of displacement boundaries, FLAC3D doesn't directly control displacements. Instead, boundary velocities are prescribed over a certain number of steps to achieve a desired displacement. If the desired displacement is "d," a velocity "v" is applied over "n" steps (where "n=d/v"). To maintain stability, it's advisable to use small velocities and a large number of steps to minimize system shocks. Commands like "zone face apply," "zone gridpoint fix," and "zone gridpoint initialize" are used to specify velocities, and gradients can also be defined. Velocities can be applied in either global or local axes.

Initial conditions

refer to the state of the model at the simulation's start. They encompass variables like stress, displacement, pore pressure, and temperature. Engineers set these values within the model domain before any external influences come into play. For instance, initial stresses can represent existing conditions, aiding subsequent stress change analysis. Initial displacements establish starting positions

for nodes or gridpoints, essential for construction or excavation scenarios. Pore pressure and temperature conditions are crucial for simulating fluid flow or thermal effects.

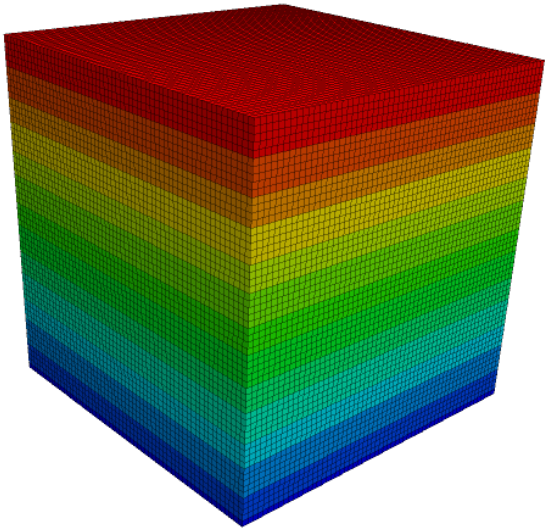

Figure 2-23 model stress state after initialization condition

These conditions interact with boundary conditions, ensuring a model's accurate response to external forces. In dynamic simulations, initial conditions evolve over time, necessitating consideration of their changes. Properly defining initial conditions is vital for simulation accuracy and stability. Consequently, Sensitivity analysis involves varying these conditions to assess their impact, enhancing the analysis's robustness. In summary, initial conditions lay the foundation for geomechanics simulations in FLAC3D, guiding how geological materials and structures behave under diverse circumstances.

Reaching equilibrium

achieving 'equilibrium' is synonymous with reaching a fully converged static solution. This state of equilibrium is typically attained through the utilization of the 'model solve' command, which allows the cycling process to continue until specific predefined limits are met. FLAC3D offers various methods to assess and visualize the proximity to convergence or equilibrium within your model. Having a comprehensive understanding of these considerations contributes to the efficiency and accuracy of your simulations. Equilibrium can be assessed based on criteria such as Maximum Out-of-Balance Force, Local Force Ratio, Average Force Ratio, Maximum Force Ratio, and Convergence. Each criterion employs its own calculation to determine convergence. If convergence criteria are not explicitly defined for a 'model solve' command, the default ratio is set at 1e-5.

FISH: the scripting language

An embedded programming language within the FLAC3D, allowing users to interact with models and customize them. With FISH, users can create new variables and functions to enhance, control, or extend program functionalities. Its versatility enables tasks like plotting variables, parameterizing models, running models, generating outputs, result monitoring, and post-processing. It was developed in response to user demands for performing complex operations that were challenging with existing program structures. Instead of adding specialized features, FISH was introduced, enabling users to write custom analyses functions. Even those without programming experience can learn to use FISH effectively, thanks to tutorials. However, FISH programs can become intricate.

```
;
fish define Run_2

    loop n (1,10)

    local Relax_2 = math.abs(gp.disp.z(gp.near(Xc,wf,4.5)))

    if Relax_2 <= 1e-4
command
mod cyc 2

end_command
    end_if
    end_loop
end
@Run_2
```

Figure 2-24 typical fish code illustrating a loop for displacement control

Constructing FISH functions incrementally and testing them on simple datasets is crucial, as FISH offers less error-checking than typical compilers. These programs are embedded in data files, with lines following "fish define" processed as a FISH function, ending when "end" is encountered. Functions can call other functions in any order, provided they are defined before usage. Saving a model also saves the compiled FISH functions and their associated variables.

3. Case study Background

The referenced work forms part of a larger project associated with an underground line, which cannot be explicitly named due to confidentiality reasons. This project encompasses various elements, including tunnels, underground spaces like cross passages, stations, wells, stub tunnels, and train manoeuvring areas, as well as surface-level auxiliary civil works. The tunnel comprises a natural section spanning 11,250.8 meters and two artificial sections corresponding to the two entrances. The total length is 49.4 meters for the (1) side entrance and 38.4 meters for the (2) side entrance. This

project involves the use of two tunnel boring machines (TBMs) originating from entrances on both the two sides. The (1) side departure involves extending the tunnel traditionally to accommodate a double-track section. Starting from the (2) side entrance, situated at an elevation of 310 meters above sea level, the route descends with a gradient of approximately 3‰ until it reaches the (1) side entrance, located at an elevation of 349 meters above sea level. The tunnel route includes sections with low coverage, and mechanized excavation methods are employed for digging. The maximum coverage distance is approximately 500 meters.

Figure 3-1 Section design showing part the geotechnical profile (Pini group).

Stratigraphy Formation	**C**	**Surface piezometer**	**γ**	C'_k	ϕ'_k	v	E'	K_0
[-]	[m]	[m]	[kN/m³]	[kPa]	[°]	[-]	[MPa]	[−]
TRV	620	105	22	600	31	0.3	3900	1

Figure 3-2 Subsoil geotechnical parameters

3.1. Studied section and construction procedure

The specific section under analysis spans 5.5 kilometres, where a metro line runs through a tunnel comprising two tubes connected by 13 cross passages. Tunnel excavation is performed using two double shield Tunnel Boring Machines (TBMs), which pass through two previously constructed stations and two shafts. The prefabricated segmental lining features an internal diameter of 9000mm and comprises 6 "universal" type segments (figure 3.2 and 3.2), referred to as 6+0, each with an average width of 1.7 meters.

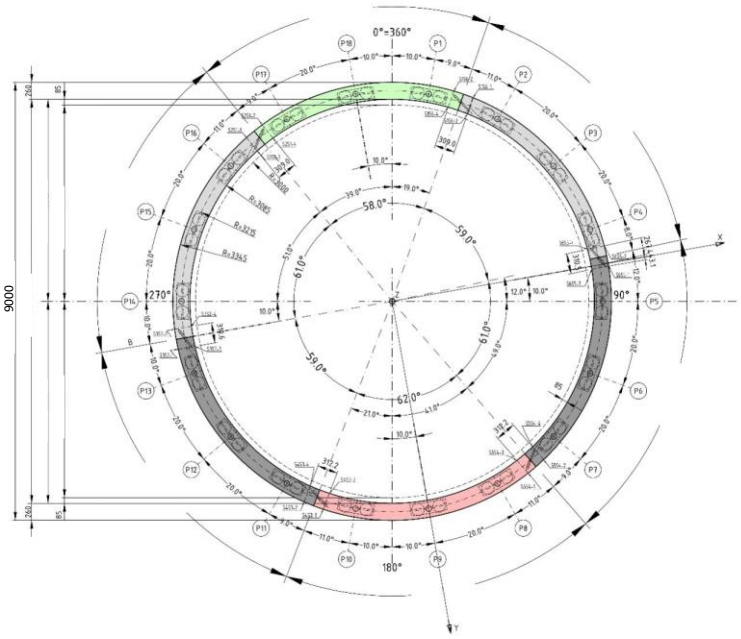

Figure 3-3- Segmental lining geometry (Pini Group)

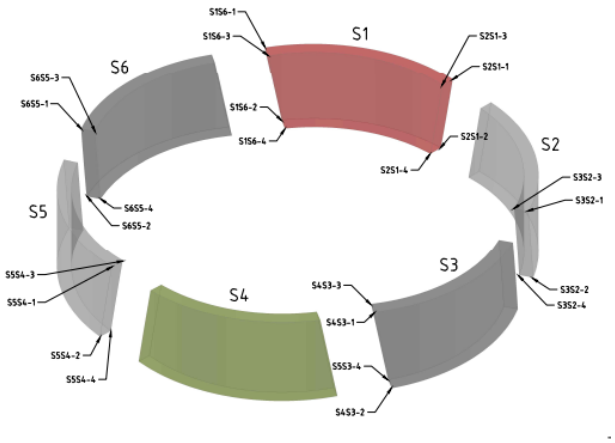

Figure 3-4– illustration of the ring (Pini Group)

Concerning the construction procedure, a temporary steel support will be employed within the fully excavated tunnel to prevent excessive stress conditions in the exposed rings and minimize ring deformations resulting from the creation of the opening. This temporary steel support will remain in place throughout the entire cross-passage construction process and will be removed once the construction is finalized. In contrast to the conventional approach of creating the opening by cutting the concrete segments, specially designed steel segments will be pre-installed (instead of the typical precast concrete segments) to facilitate a faster and more straightforward opening formation. The opening will be established by disassembling the central portion of the steel segment, while the remaining outer part of the steel segments will serve as a portal frame,

supporting the hoop load from the exposed rings. The excavation work will employ a sequential excavation method, often referred to as the New Austrian Tunnelling Method (NATM). Temporary support will involve the use of shotcrete, wire mesh, and lattice girders. Once excavation is completed in each cross-passage, a permanent concrete lining will be cast.

Characteristics	Universal ring ashlars
Thickness of concrete segments	50cm
Number of segments	6
Average ring width	1.7
Segment reinforcement type	SFRC
Characteristic compressive strength	50MPa
Characteristic tensile strength	5MPa
Characteristic flexural strength	5.2MPa
Elastic module	34800 MPa

Table 3-1 Material properties of concrete precast segment

4. Methodology

The analysis of this study is composed of three components: (1) modelling excavation sequence for the 3D FDM and extraction of segmental lining resultant forces and creation of a corresponding SSM (shell-spring model) with help of analytical solutions, (2) compatibility check between the FDM and SSM and Analysis of stress redistribution due to the formation of the cross-passage openings using FEM and SSM, (3) incorporation of circumferential and longitudinal joints in both models, and (4) design of temporary steel support system.

4.1. 3D finite difference model and 3D shell-spring model

Rather than embarking on the ambitious task of modelling the entire length of the tunnel, a decision was made to focus on a constrained section. This decision was rooted in practical considerations, primarily cantered on the substantial computational time and memory space required for a comprehensive model. In this endeavour, both the 3D Finite Difference Method (FDM) and the 3D Stress-Stiffness Method (SSM) were employed. However, it's worth noting that the boundaries of our selected model section were thoughtfully extended to ensure that any boundary-related interference with the calculations was effectively eliminated.

As visually represented in Figure 4.1, a deliberate choice was made to subject Rings 4 and 5 to a partial opening, resulting in a cross-sectional area measuring 17.8 square meters. Notably, certain structural elements were intentionally excluded from our modeling efforts. Specifically, we neglected to account for the temporary steel support and the permanent concrete lining. This deliberate omission aligned with the primary objective of our analysis, which was to investigate the complex phenomenon of stress redistribution occurring within the tunnel lining in response to the introduction of a cross-passage.

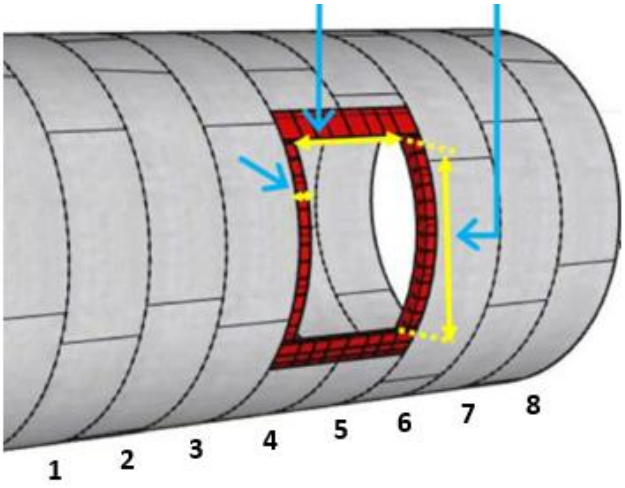

Figure 4-1simplified layout of Cross passage opening.

To facilitate the modelling process, a simplification technique was employed. Initially, the tunnel lining was conceptualized as a continuous cylinder, a step taken to enable more manageable computational analysis. However, it is essential to emphasize that, in subsequent phases of the study, we delved into the behaviour of the tunnel lining, paying specific attention to the presence of segmental joints. This analysis of joint behaviour played a pivotal role in our endeavour to attain a comprehensive understanding of the structural dynamics. Furthermore, our research extended beyond the examination of the tunnel lining's response to joints. We also embarked on a rigorous comparative analysis, leveraging the insights derived from both the 3D Finite Difference Method (FDM) and 3D Stress-Stiffness Method (SSM) models. This comparative approach allowed us to discern subtle nuances and variations in stress distributions, thereby enriching the depth and rigor of our study. Lastly, it's worth noting that, as an integral part of this research, we undertook the design and subsequent analysis of the steel frame within the context of both modelling methodologies. This aspect of our study contributed essential insights into the structural stability and performance of the tunnel lining under various conditions and configurations.

4.2. 3D FDM

A 3D numerical model was meticulously constructed utilizing the commercial software package FLAC3D, which leverages the versatile Generalized Finite Difference Method (FDM). Throughout the development of this model, painstaking attention was devoted to assessing the ramifications of boundaries and mesh discretization. In specifying the dimensions of the 3D model, it was defined as having equal width, length, and height, each spanning 100 meters. In order to safeguard against the undue influence of boundary conditions on the simulation outcomes, a prudent strategy was employed. Monitoring of the lining loads was conducted at a distance approximately four times the tunnel diameter (4D) away from the model boundary. This strategic placement of monitoring points ensured that the effects of boundary conditions remained inconsequential within the region of interest. Furthermore, it was deemed imperative to extend the simulation of tunnel excavation beyond the confines of the monitored rings. This extension was necessitated by the observation that the impact of the tunnel face on the model diminished to a negligible level at a distance exceeding 2.5 times the tunnel diameter (2.5D). This extension was a crucial component of our modeling approach, enabling a comprehensive exploration of the tunnel excavation process and its effects. The initial state of the model was established with a lateral earth pressure ratio denoted as K_0 = 1, as depicted in Figure 4.2. This parameterization served as the foundational starting point for our numerical simulations, providing a baseline against which subsequent alterations and responses could be evaluated.

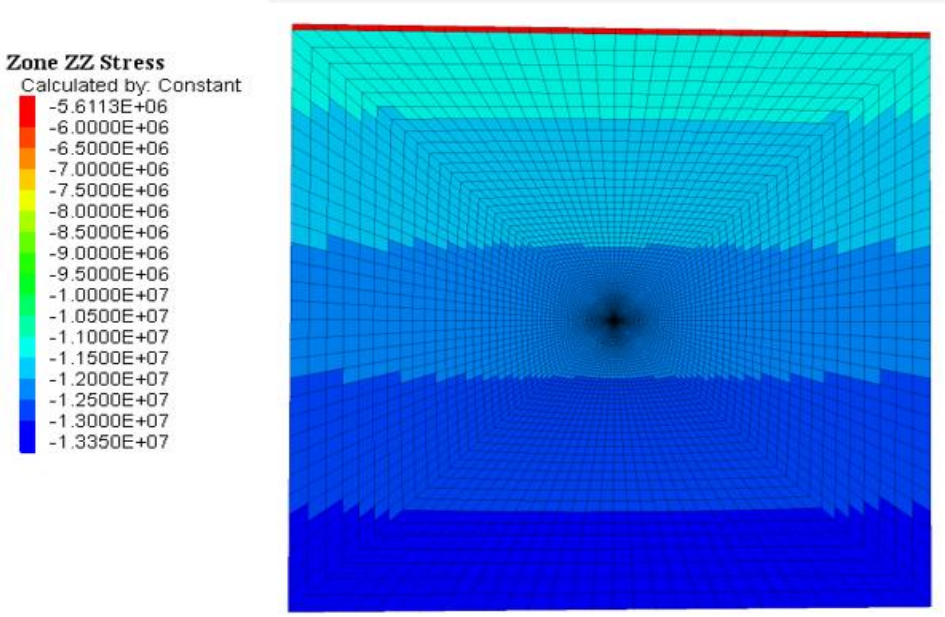

Figure 4-2 state of stress after initialization

To ensure an accurate representation of face pressure within our framework, we implemented a trapezoidal distribution of horizontal stress at the tunnel face. This modeling approach aligns with

established methodologies found in prior research studies (Do, Dias, & Oreste, 2015; Do et al., 2014a; Kasper & Meschke, 2004, 2006). By doing so, we aimed to faithfully capture the dynamic pressures encountered during the process of tunnel excavation. To simulate the Tunnel Boring Machine (TBM) shield, we employed a conical shape constructed using shell elements. The shield was divided into three distinct sections, each characterized by a progressive reduction in Young's modulus to account for its conical geometry. This segmentation enabled us to accurately represent the nuanced differential movements of the soil surrounding the rear shield, in contrast to the ground adjacent to the front shield.

Incorporating the jacking forces into our model involved the direct application of concentrated forces to the nodes situated at the edges of the shield segments. This method effectively mirrored the forces exerted during the excavation process, enhancing the accuracy and fidelity of our simulations. Furthermore, to account for the gravitational effect on the shield itself, we applied vertical loads along the tunnel invert, spanning the entire length of the shield and oriented orthogonally at 90 degrees to the tunnel axis. This approach is consistent with established practices observed in prior research (Do et al., 2014a; Hasanpour, 2014) and ensured that the self-weight of the shield was faithfully represented within our model.

Additionally, we meticulously addressed the impact of the back-up train weight by applying distributed forces to the lower sector of the lining. These forces covered 90 degrees of the lining's circumference along the length of the back-up train. This comprehensive approach allowed us to consider and account for the dynamic loading conditions associated with the presence of the back-up train, thereby enriching the depth and authenticity of our analysis.

4.2.1. Modelling the tunnel lining

The segmental lining is represented using linear-elastic embedded liner elements provided by Itasca (2009). These liner elements have a shell-like shape and are equipped with two links at each node, facilitating interaction between the surrounding medium (ground) and the structural element on both sides. One end of the embedded liner element connects to the surrounding ground, while the other end links the two adjacent segments. Regarding the interface between the liner and the surrounding soil, conventional analytical solutions typically assume one of two extreme conditions: full-slip, where there is no transfer of tangential stress between the liner and the ground/grout, or no-slip, allowing for the transfer of shear tangential stress between the liner and the ground/grout, as proposed by Rankin et al. (1978). However, in numerical analyses of ground-structure interaction, it is possible to model this interface using frictional contact. In such cases, a zero coefficient of friction implies no transfer of tangential shear stress between the

lining and the ground, similar to the full slip condition (as described by Sedarat et al. in 2009). The study introduces a more nuanced approach for the lining-ground interface conditions by assuming no-slip with a relatively high friction angle, which permits the transfer of tangential stress between the liner and the ground. The frictional contact model incorporates a linear-elastic link between the soil and the liner for shear stresses below the allowable shear strength, as defined by the Mohr-Coulomb failure criterion. This linear-elastic link, marked as (1) in 4.3 b, allows sliding and opening relative to the surrounding ground and is assigned a stiffness based on a widely accepted rule of thumb. Specifically, the normal stiffness (kn) and tangential stiffness (ks) are set at values one hundred times the equivalent stiffness of the neighbouring zone (the surrounding ground). It's essential to note that this model does not consider the presence of grout as a material with elastic behaviour, and the simulation of grout itself has been omitted, as it is not the primary focus of the current study.

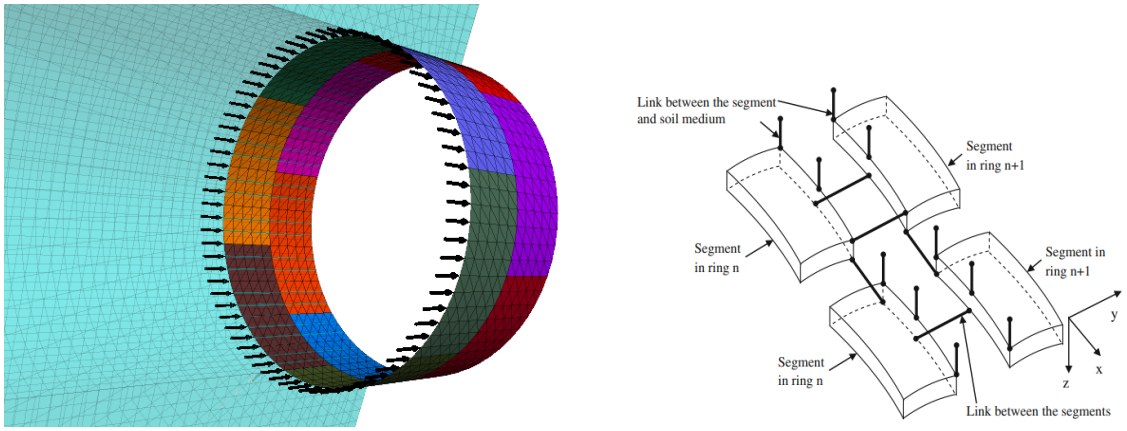

(a) (b)

Figure 4-3 . (a) segmental lining and applied jacking force, (b) Ring joint scheme

4.3. 3D SSM

The 3D shell-spring analysis was executed utilizing the SAP2000 software program. In this analytical framework, we represented the tunnel segments through the use of four-node quadrilateral shell elements. Since these shell elements operate in a planar context, our approach involved subdividing the tunnel lining into a series of smaller elements, effectively capturing the complete circular configuration of the tunnel lining. To simulate the intricate interaction between the tunnel lining and the surrounding ground, we introduced a system of radial springs and tangential springs, collectively referred to as "ground springs." These springs were strategically attached to each element along the circumference of the tunnel lining ring. The radial springs were affixed to replicate the normal stresses induced by the outward deflection of the tunnel lining, while the tangential springs were employed to

simulate the shear stresses arising at the interface between the tunnel lining and the adjacent ground. Notably, we opted to exclude springs under tension, a choice that aligned with our objective of faithfully replicating the actual behaviour of the tunnel lining under the specified conditions.

In this study, the specific constants associated with the radial and tangential springs were determined employing equations that had been proposed by Duddeck and Erdmann [15]. These equations provided a robust basis for accurately calibrating the stiffness of these springs, ensuring the fidelity of our model in replicating the real-world behaviour of the tunnel lining and its interaction with the surrounding ground.

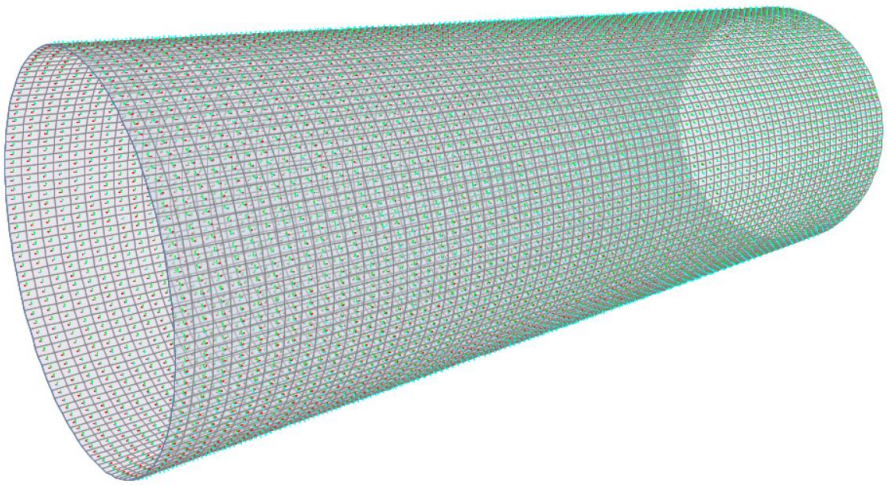

Figure 4-4 . illustration of SSM within the structural software SAP2000

To model the ground springs in the analysis, area springs were employed. Both the vertical and horizontal ground pressures acting on the tunnel lining were considered as uniformly distributed loads. However, here the external radial loads acting on the lining were derived simply using Mariottes or Barlow formula, this was done by retrieving the the radial pressure that resulted in the axial forces in the tunnel lining within the 3D FDM. Its worth to note that, applied pressure can be retrieved simply from a 2D numerical model, and that 3D models are not needed.

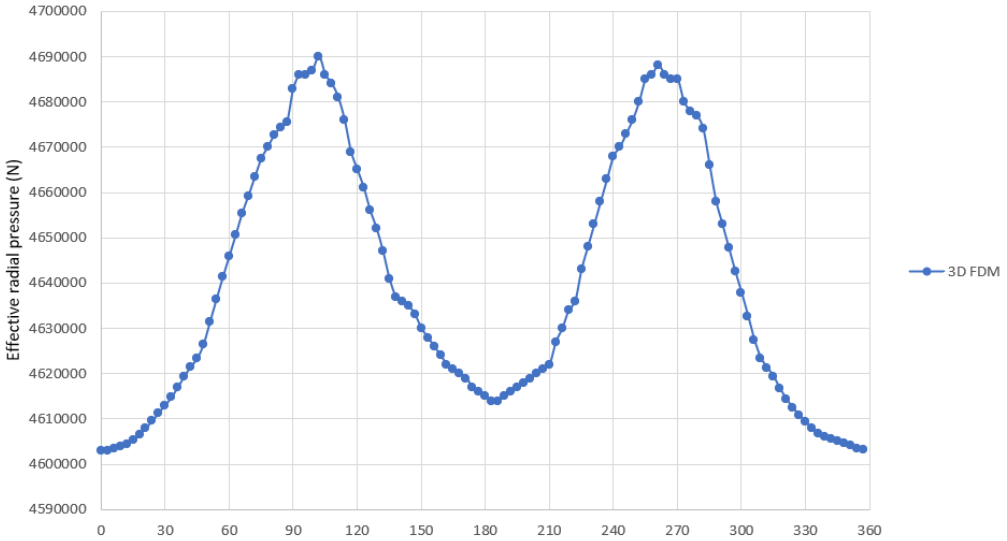

Figure 4-5 distribution of radial load within the SSM

4.4. Creation of the opening

The most crucial phase of the construction process involved removing the segments to create the openings. As the construction of the cross-passages commenced, the integrity of the tunnel lining improved to some extent because the cross-passage structure provided support to the main tunnel. Once the cross-passages were completed, they contributed to reducing the ovalization of the segmental lining by offering lateral resistance to the bored tunnel. Additionally, the induced axial forces in the segmental lining decreased due to the transfer of axial forces from the segmental lining to the cross-passage lining. To simulate the most critical construction phase, construction sequence was assumed in the two models, as outlined in tables 4.1 and 4.2.

Stage	***Description***
I	Initial stress conditions obtained according to k0 value.
II	Thick material with higher density was added at the top model boundary to compensate for increased tunnel depth.
III	Tunnel excavated and lining installed simultaneously according to TBM advancement sequence.
IV	Cross passage opening created by deleting liner element using 'structure delete' command.

Table 4-1 construction phases within 3D FDM

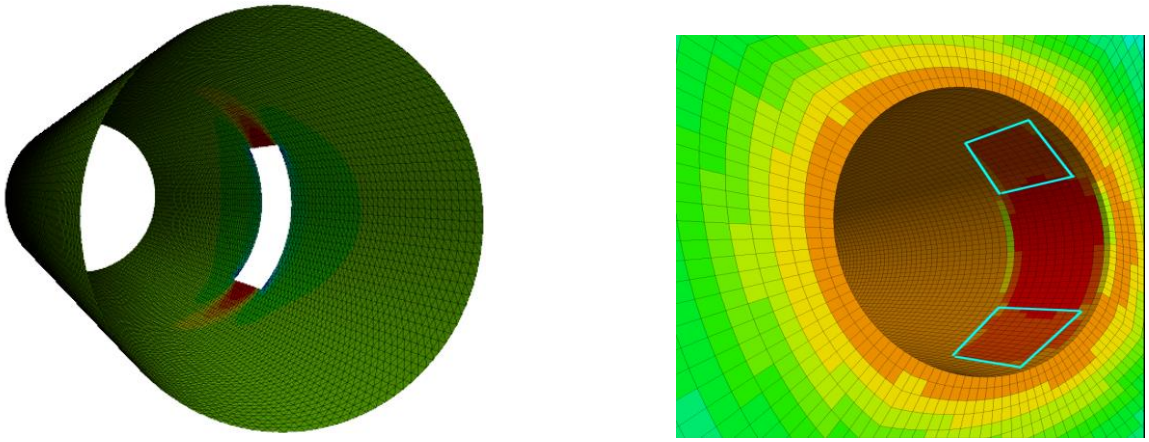

(a) *(b)*

Figure 4-6 (a) continues lining after opening (FDM), (b) illustration of zones of stress reduction.

Stage	***Description***
I	Creation of cylindrical shell accounting for same lining mesh and properties of the FDM.
II	Introduction of the radial and tangential ground springs (Duddeck and Erdmann).
III	Uniform inward shell radial pressure
IV	Creation of the opening by deleting the shell area section. Reduction of external load to account for stress redistribution after the opening.

Table 4-2 construction phases within 3D SSM

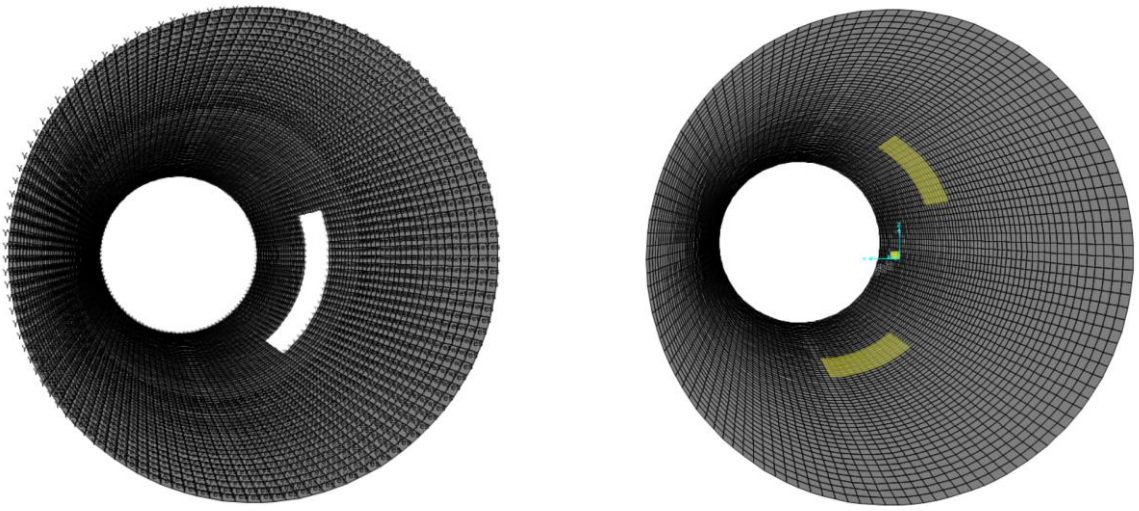

(a) **(b)**

Figure 4-7 (a) 3D SSM with cross passage opening, (b) area subjected to load reduction.

4.5. Introducing the longitudinal and circumferential joints

In the 3D Finite Difference Model (3D FDM), as previously discussed in section 4.2.1, the tunnel lining comprises two links: one that connects to the ground and another to the adjacent segment. Adhering to the methodology outlined by Do et al. (2013b), it's important to note that each link within the embedded liner element is endowed with six degrees of freedom. These degrees of freedom can be assigned one of three distinct boundary conditions: free, rigid, or deformable. These boundary conditions are essentially represented as six springs, encompassing three translational components identified as K_{R} and K_{A} in Figure 4.8b, as well as three rotational components denoted as K_{θ} in Figure 4.8b.

4.5.1. Segment joints

The segment joints in our analysis were simulated using double node connections, as illustrated in Figure 4.3b. These connections encompassed six degrees of freedom, which were represented by six springs. Specifically, there were three translational components in the x, y, and z directions and three rotational components along the x, y, and z directions, with respect to the global coordinate system.

These springs were assigned stiffness values based on one of four attachment conditions: Free, Linear spring with a specified stiffness factor, Bi-linear spring characterized by both a stiffness factor and a yield strength or Rigid the stiffness characteristics of the joint connection were represented by a set consisting of a rotational spring (, K_{θ}), an axial spring (K_{A}), and a radial spring (K_{R}), as depicted in Figure 4.8b.

The behaviour of axial springs was approximated using a linear relation based on empirical data and a constant coefficient spring. On the other hand, the radial stiffness and rotational stiffness of a segment joint were modelled using a bi-linear relation, which included a stiffness factor and a maximum bearing capacity. For all investigated cases, the translational component in the y-direction (parallel to the longitudinal axis of the tunnel) and two rotational components around the x and z directions were assumed to be rigid. The values of the spring constants used to simulate the segment joints were determined based on simplified procedures presented in studies by Thienert and Pulsfort and Do et al. Further discussion on the justification and the impact of using simple linear or bi-linear springs to represent segment joint behaviour can be found in the study conducted by Do et al. The specific spring constants utilized in our analysis can be found in Table 4.3.

Segment joints	Value	Ring joints	Value
Rotational stiffness K_θ (MN m/rad/m)	100	Rotational stiffness $K_{\theta R}$ (MN m/rad/m)	100
Maximum bending moment at segment joint M_{yield} (kN.m/m)	150	Maximum bending moment at ring joint M_{Ryield} (kN.m/m)	150
Axial stiffness K_A (MN/m)	500	Axial stiffness K_{AR} (MN/m)	500
Radial stiffness K_R (MN/m)	1,050	Radial stiffness K_{RR} (MN/m)	1,050
Maximum shear forces at segment joint S_{yield} (MN/m)	0.55	Maximum shear forces at ring joint S_{Ryield} (MN/m)	0.55

Table 4-3 parameters of joints in present model

4.5.2. Ring joints

As described in the works of the same authors, the ring joint has also been simulated using double connections Fig. 4.3 b. In this study, the rigidity characteristics of the ring joint connection have been represented by a set composed of a rotational spring ($K_{\theta R}$), an axial spring (K_{AR}) and a radial spring (K_{RR}), as depicted in Fig.4.8 b. The interaction mechanism of each spring is the same as the one applied for a segment joint. The attachment conditions of the translational component in the x direction (tangential to the tunnel boundary) and two rotational components around the y and z directions have been assumed to be rigid for all the investigated cases. The other parameters of the ring joints are summarized in Table 4.3

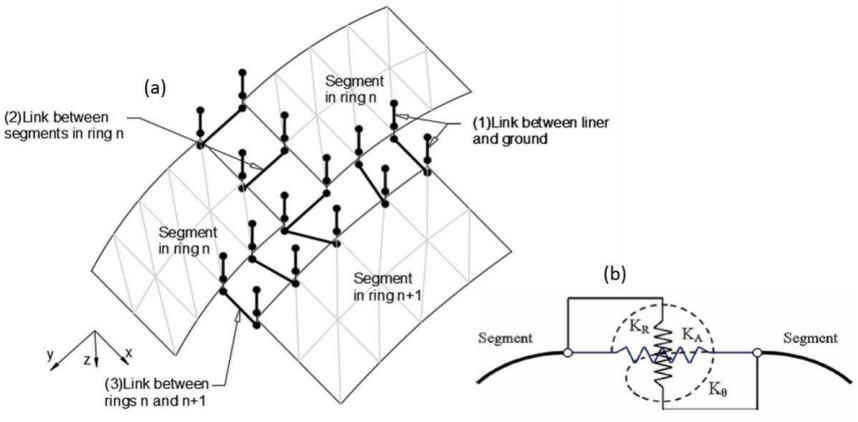

Figure 4-8 Segmental lining modelling concept (a) node connectivity concept (after Do et al. 2013a), (b) K_R, K_A, K_θ stiffness in the axial, radial and rotational directions of a ring joint (Do et al. 2013a)

In contrast, the 3D Shell-Spring Model (3D SSM) representation of the circumferential and longitudinal joints was done by applying edge releases to the shell element edges, assigning edge releases with partial fixity springs holding properties similar properties to the links recommended by Do et al.(2013b). This process is straightforward and can be accomplished using the "Assign" menu command for shell elements, making it a convenient method for assigning simple supports to shells.

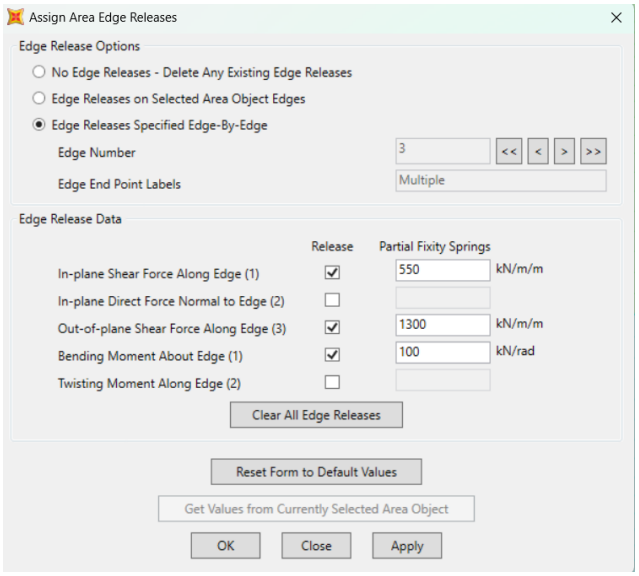

Figure 4-9 edge release window (SAP2000)

4.6. Design of temporary steel frame

Taking into careful consideration the forces exerted upon the tunnel lining and accounting for the specific ground conditions, groundwater levels, and the dimensions of the planned openings, a meticulous evaluation process guided our decision to implement a steel-based temporary support system. This system was meticulously engineered to provide comprehensive internal support, covering the entire 360° circumference of the tunnel lining. This comprehensive coverage extended to both the sections with openings and the adjacent fully enclosed rings. The core of this support system consisted of five interconnected steel rings, thoughtfully linked together by longitudinal beams. However, in regions corresponding to the openings, we opted for a strategic combination of steel arcs and steel columns instead of employing complete steel rings. This strategic choice was made with the primary objective of significantly enhancing the overall stiffness of the support structure, thereby minimizing any additional deformations that might arise within the segmental lining due to the creation of these openings. A pivotal aspect of this design was ensuring the efficient transfer of loads from the tunnel structure to the support system. To achieve this, we attached the steel cage securely to the intrados of the tunnel lining. This secure attachment was accomplished through the application of a 50 mm thick cement mortar layer, as visually represented in Figure 4.10.

By carefully considering the intricacies of the tunnel structure, the support system, and the specific load-bearing requirements, we aimed to provide a robust and reliable solution that would effectively withstand the dynamic forces and deformations inherent in tunnel construction under the given conditions.

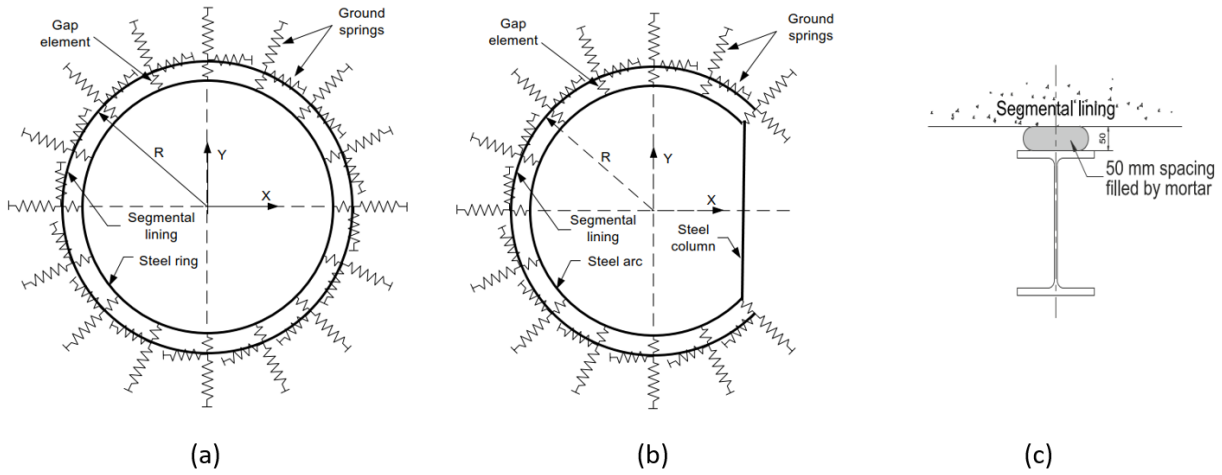

Figure 4-10 Components of the temporary support system: (a) opened ring section, (b) closed ring section, and (c) packing agent.

In the context of the 3D Shell-Spring Model (3D SSM), we carefully introduced gap elements to faithfully replicate the characteristics of the mortar layer. These gap elements, specifically engineered to activate solely under compression, serve a vital role in emulating the behavior of the mortar layer within the support system. The precise stiffness characteristics of these gap elements were meticulously determined in accordance with the guidelines and recommendations outlined by Yang et al. [36]. This rigorous approach ensured that the gap elements closely mirror the anticipated performance of the actual mortar layer. This attention to detail and precision in design underscores our unwavering commitment to achieving optimal support and minimizing structural deformations throughout the construction process. By incorporating these gap elements into our model, we aim to simulate the crucial role played by the mortar layer in providing stability and load transfer within the support system, further enhancing the accuracy and reliability of our simulations.

$$k = \frac{E_m A_m}{t} \qquad (4.1)$$

Where E_{m} is the elasticity modulus of the mortar material, A_{m} is the effective area of a single spring, and t is the thickness of the mortar layer.

On the other hand, an actual gap between the steel frame and the lining is not required within the 3D FDM model, as the steel support was simulated using the beam structural element which

connects directly to the lining through the element nodes, the linking between the beam and the liner element followed the same stiffness suggested by equation 4.1.

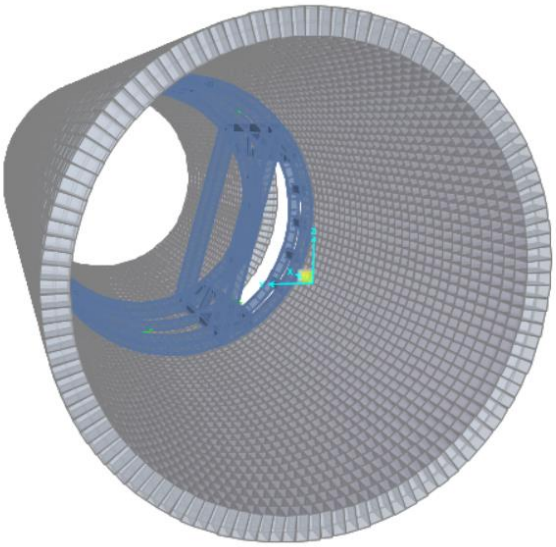

Figure 4-11 temporary steel support within the SSM

4.7. Comparison of member forces

The comparison of induced axial and longitudinal forces, as well as bending moments in the tunnel lining, was conducted both before and after the creation of a cross-passage opening. To achieve this, member forces in the longitudinal and tangential directions to the tunnel lining, along with the bending moments, were extracted from both the 3D Finite Difference Model (3D FDM) and the 3D Shell-Spring Model (3D SSM). The comparison was initially performed for a continuous liner, which can be visualized as a tube-like element characterized by uniform rigid links along the entire length without any discontinuities. Subsequently, longitudinal and circumferential joints were introduced in both models, and another round of comparison was conducted. This step allowed us to evaluate the impact of joints on the behaviour of the tunnel lining. Lastly, to further explore the effects of joints on lining behaviour, we compared the continuous lining with the segmental lining. This comparative analysis provided valuable insights into how the presence of joints influenced the overall response of the tunnel lining.

It is essential to note that this comparison was conducted using both graphical representations and quantitative measures. The quantitative comparative analysis was executed using specific equations designed to assess and quantify the differences between the results obtained from the two modelling approaches. This comprehensive evaluation approach ensures a thorough understanding of the variations in tunnel lining behaviour under different conditions and configurations.

$$R_N^2 = 1 - \frac{\sum(N_{SSM,i} - N_{FDM,i})^2}{\sum(N_{SSM,i} - \overline{N_{SSM}})^2}, \quad (4.2)$$

where

$$\overline{N_{SSM}} = \frac{1}{n}\sum_{i=1}^{n} N_{SSM,i} \quad (4.3)$$

$$R_F^2 = 1 - \frac{\sum(F_{SSM,i} - F_{FDM,i})^2}{\sum(F_{SSM,i} - \overline{F_{SSM}})^2}, \quad (4.4)$$

where

$$\overline{F_{SSM}} = \frac{1}{n}\sum_{i=1}^{n} N_{SSM,i} \quad (4.5)$$

$$R_M^2 = 1 - \frac{\sum(M_{SSM,i} - M_{FDM,i})^2}{\sum(M_{SSM,i} - \overline{M_{SSM}})^2}, \quad (4.6)$$

Where

$$\overline{M_{SSM}} = \frac{1}{n}\sum_{i=1}^{n} M_{SSM,i} \quad (4.7)$$

Where R_N^2, R_F^2 and R_M^2 refer to the overall coefficients of determination for axial forces (N), Longitudinal forces (F) and bending moments (M), respectively. This indicates the global fit between the member forces derived from 3D SSM and 3D FDM.

4.7.1. Continues lining.

The two models were further investigated after the creation of the cross passage opening. To do so, member force from three different cross sections were extracted and analysed. Cross Section 1 (CS 1) corresponds to a plane at the centre of the cross passage opening. CS 2 corresponds to a plane located at the unopened adjacent ring to the cross passage opening (0.15 m from the opening). CS 3 corresponds to a plane located at the unopened adjacent ring (1.5 m from the opening.).

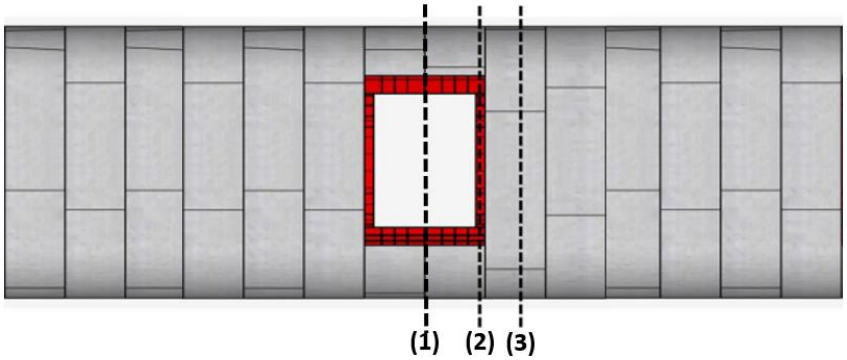

Figure 4-12 selected cross sections for member forces comparison

4.7.2. Segmental lining

To assess the effect of longitudinal and circumferential joints on the induced member forces in the tunnel lining, a comparative analysis for member forces extracted from the 3D FDM was made before the creation of the cross passage opening. To do so two cross sections were taken as illustrated in 4.13 where CS1 corresponds to a plane that passes through the middle of a ring along the tangential direction of the tunnel lining and CS2 corresponds to a plane passing through the lateral boundary of the same ring.

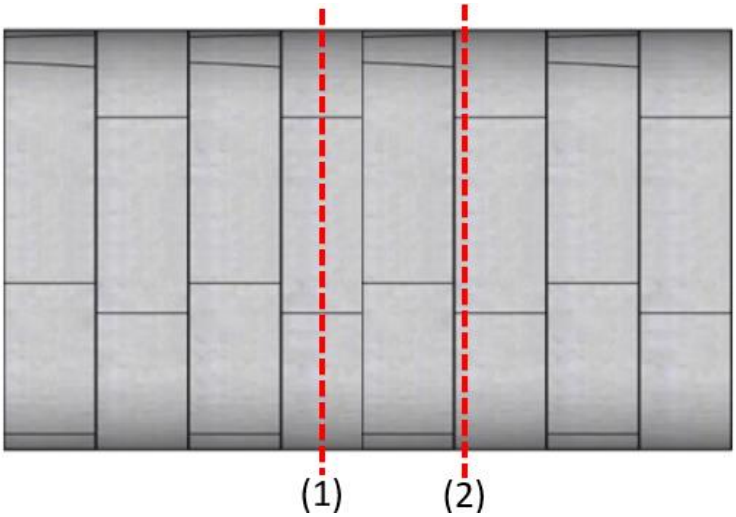

Figure 4-13 selected cross section for member forces comparison

4.7.3. Temporary steel support

The investigation into the structural response of the tunnel lining, with and without the installation of the temporary support system, entailed a thorough comparison of the member forces obtained from two distinct analyses. The first analysis was conducted using the 3D Shell-Spring Model (3D SSM) with the temporary support system in place. The second analysis involved the 3D shell-spring analysis, but this time, it was carried out without the installation of the temporary support system. To facilitate this comparison, identical cross sections, as previously mentioned in CS 1, were employed. Through this comparative study, conclusions were drawn to present a practical and conservative approach for designing tunnel lining in cross-passage sections. This comprehensive analysis allowed us to assess the effectiveness and necessity of the temporary support system in mitigating structural forces and ensuring the stability of the tunnel lining during construction. The results of this study

provide valuable insights for engineers and designers when considering the design and implementation of tunnel lining systems in similar cross-passage configurations.

5. Results

As discussed in section 4.2.1, in order to prevent the liner element from slipping at the ground-structure surface, a normal and shear coupling stiffnesses were assigned according to Itasca role of thumb that the stiffness should be 10-100 times the stiffness of the smallest zone at the interface, in order to check the non-slipping phenomena displacement of both the liner and the zone surrounding it were monitored, as the displacement difference should be as low as possible.

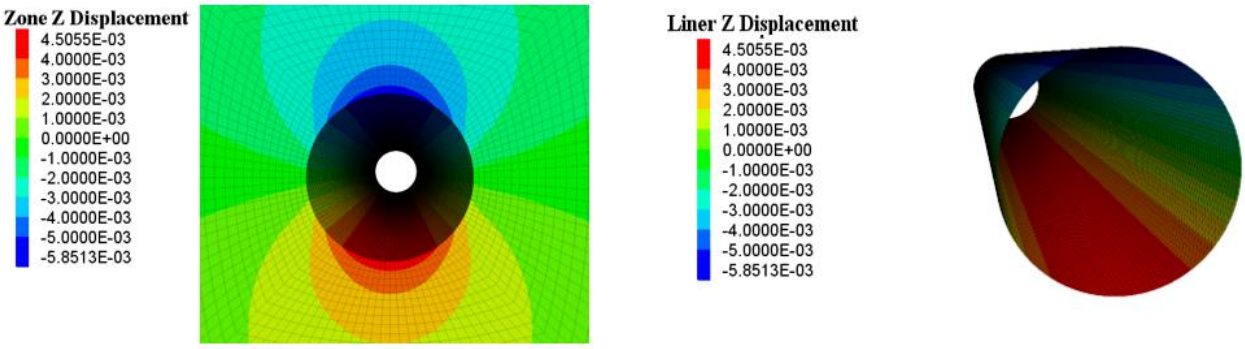

Figure 5-1 Liner and zone displacement within the 3D FDM

5.1. Continuous lining

Figure 5.2 presents a comparison of the axial and longitudinal forces obtained from both the 3D Finite Difference Model (3D FDM) and the 3D Shell-Spring Model (3D SSM). Upon close examination of the illustration, several observations can be made. In regard to Axial Forces and Bending Moments: The data reveals a noteworthy agreement between the axial forces and bending moments obtained from the 16-ring 3D SSM and those obtained from the closed ring-3D FDM. This alignment suggests that the 16-ring 3D SSM provides results that are in good accordance with the closed ring-3D FDM for these specific parameters. On the other hand, regarding Longitudinal Forces, there is a discernible trend indicating that the 3D SSM tends to overestimate the longitudinal forces when compared to the 3D FDM. This discrepancy in longitudinal forces suggests that there may be variations in how the two models capture and represent this particular aspect of the structural response.

These findings provide valuable insights into the comparative behaviour of the two modelling approaches and highlight areas where further investigation or calibration may be necessary to achieve even closer alignment between their results.

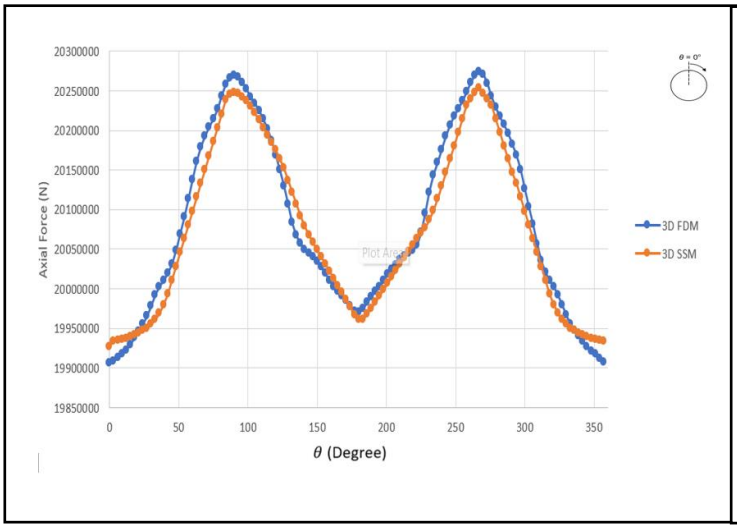

(a) axial force comparison

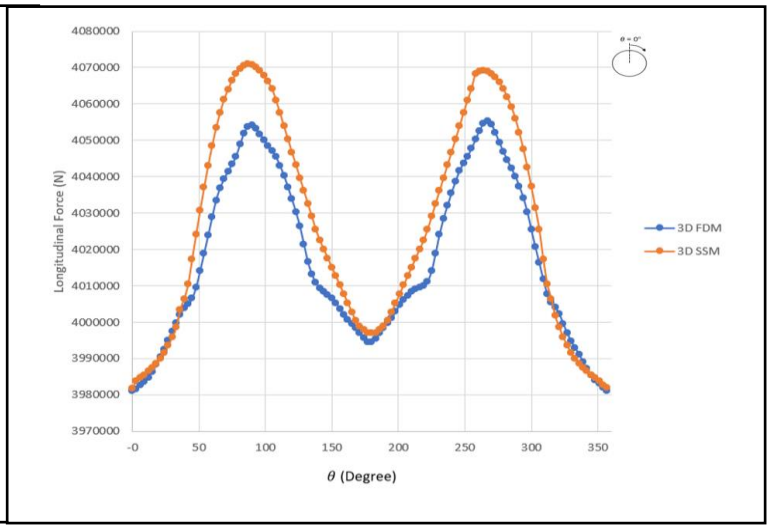

(b) Longitudinal force comparison

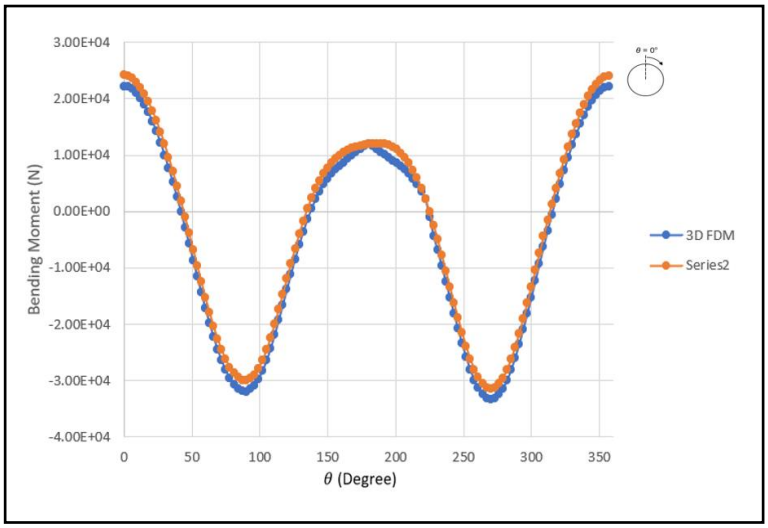

(c) bending moment force comparison

Figure 5-2 comparison of member forces in a continues lining.

In addition, Table 5.1 provides a quantitative comparison of the member forces obtained from the 3D Shell-Spring Model (3D SSM) and the 3D Finite Difference Model (3D FDM). Specifically, R_{N}^2 and $\boldsymbol{R}_M^2$, as discussed in section 4.7, represent the overall coefficients of determination for axial forces (N) and bending moments (M), respectively. These coefficients of determination, R_{N}^2 and $\boldsymbol{R}_M^2$, serve as quantitative indicators of the level of agreement or correlation between the results obtained from the 3D SSM and the 3D FDM for axial forces and bending moments. They provide a statistical measure of how closely the two modelling approaches align in terms of these critical structural parameters, aiding in the assessment of their comparative accuracy and reliability.

CS	R_N^2 for N	$\frac{N_{SSM}}{N_{FDM}}$	R_F^2 for F	$\frac{F_{SSM}}{F_{FDM}}$	R_M^2 for M	M_{SSM}/M_{FDM}
1	0.951	0.999	0.85	1.002	0.989	1.07

Table 5-1 Quantitative comparison between the 3D SSM results and 3D FDM results

In summary, the overall comparison of both models suggests a high degree of agreement in terms of the resulting member forces. Therefore, it can be confidently asserted that the developed 16-ring 3D Shell-Spring Model (3D SSM) is compatible with the closed ring-3D Finite Difference Model (3D FDM). This compatibility signifies that the 16-ring 3D SSM can effectively capture and simulate the structural behaviour observed in the closed ring-3D FDM, reinforcing the reliability and applicability of the 16-ring 3D SSM in modelling and analysing similar structural scenarios.

In the undisturbed situation, where there are no openings, the induced axial forces in the tunnel lining typically follow a circumferential path, flowing from the tunnel crown to the invert. However, with the introduction of openings, this initial axial flow path becomes disrupted, and the forces tend to redistribute, flowing around the openings. Consequently, the load is transferred to the adjacent unopened rings. Figure 5.3 provides a graphical illustration of this behaviour, and several observations can be made. first, agreement in CS1 and CS2: The member forces obtained from both the 3D Shell-Spring Model (3D SSM) and the 3D Finite Difference Model (3D FDM) show a good agreement, particularly in CS1 and CS2. These results indicate that both models accurately capture the behaviour of forces around the openings in these sections. Second Discrepancy in CS3: However, in CS3, a difference between the two models is evident, suggesting that as you move further from the opening, the behaviour of the models diverges. This indicates that the effect of the cross-passage opening on the further rings is not consistent between the two models. Third, Specific Behaviour at CS1: In particular, at CS1, it's worth noting that the resulting member forces from both models tend to concentrate more at the lateral boundaries of the opening, particularly at angles 75 and 135 degrees. Additionally, the 3D SSM depicted a slightly higher peak member force than the 3D FDM. Lastly, Quantitative Analysis in Table 5.2: The quantitative analysis in Table 5.2 further supports these observations. The overall coefficient of determination for both axial forces and bending moments at CS1 and CS2 shows a higher degree of agreement, while longitudinal forces exhibit somewhat less agreement with a value of 0.75. However, when comparing the overall average values of forces obtained from each model, all member forces tend to exhibit very good agreement.

These findings provide valuable insights into how the two modelling approaches capture the redistribution of forces around cross-passage openings. They underscore the importance of considering specific cross-sections and the potential variations in behaviour when designing tunnel linings with openings.

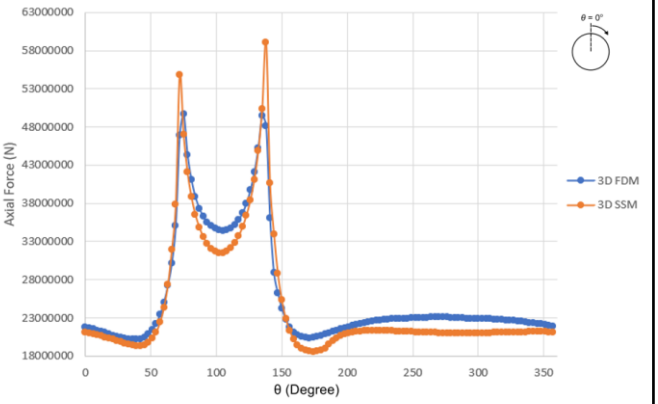

(a) CS 1 axial force comparison

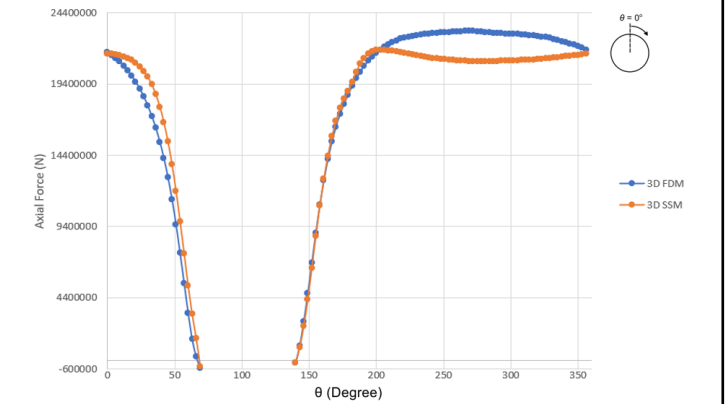

(b) CS 2 axial force comparison

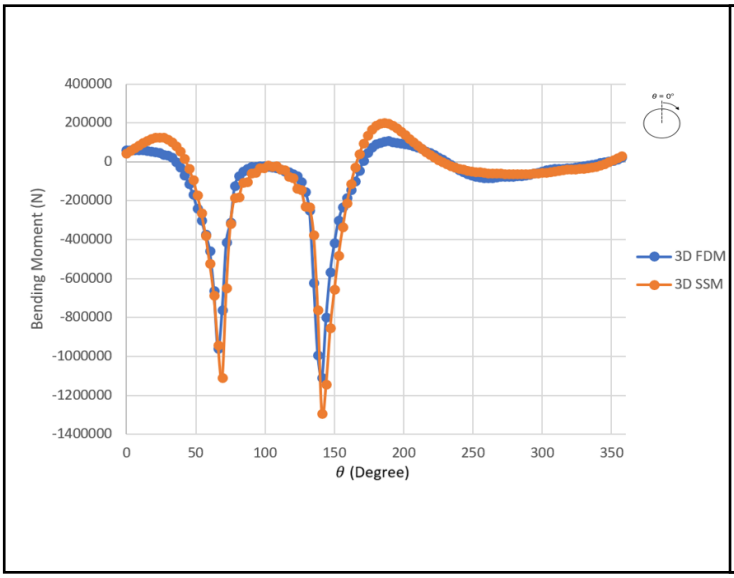

(c) CS 1 Bending moment comparison

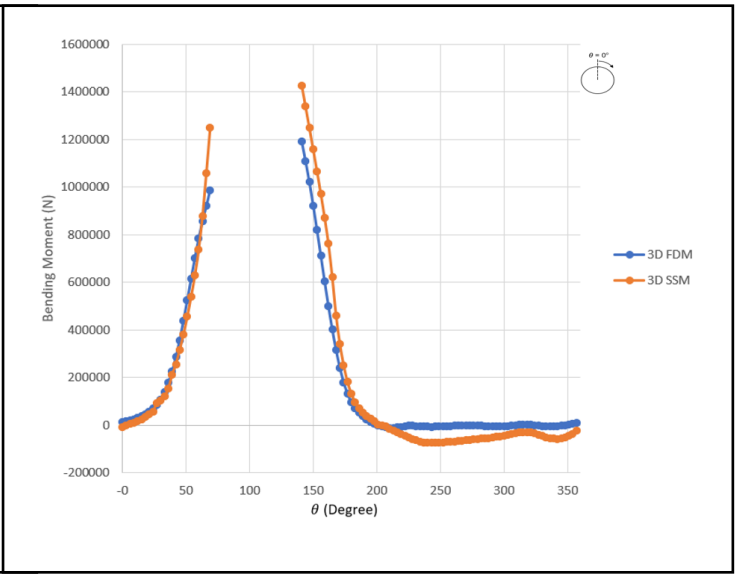

(d) CS 2 Bending moment comparison

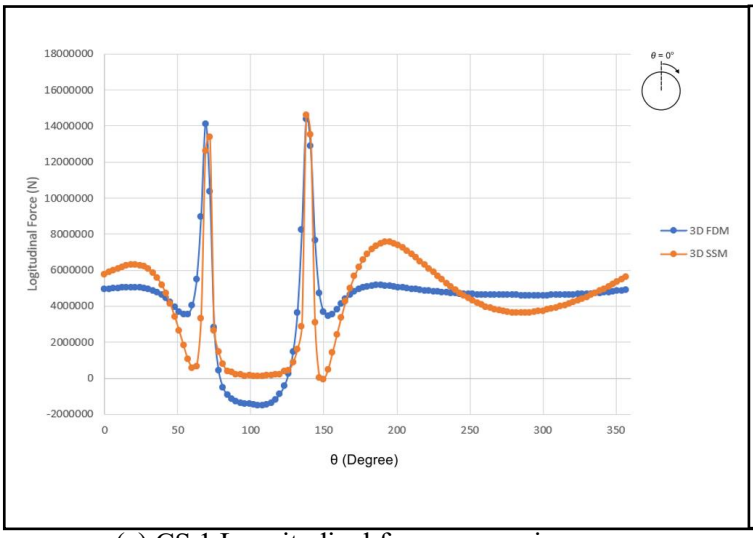

(e) CS 1 Longitudinal force comparison

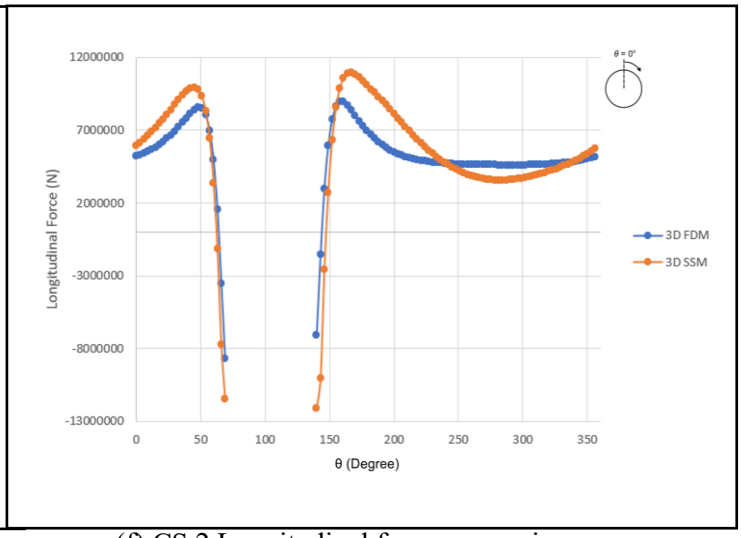

(f) CS 2 Longitudinal force comparison

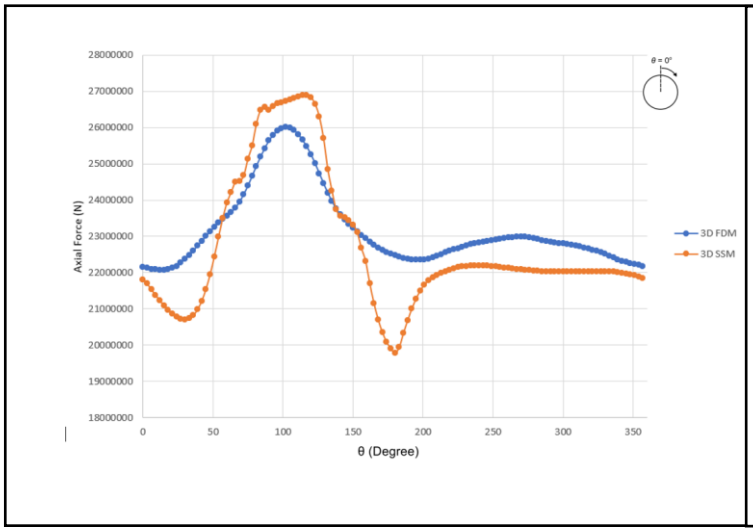

(g) CS 3 axial force comparison

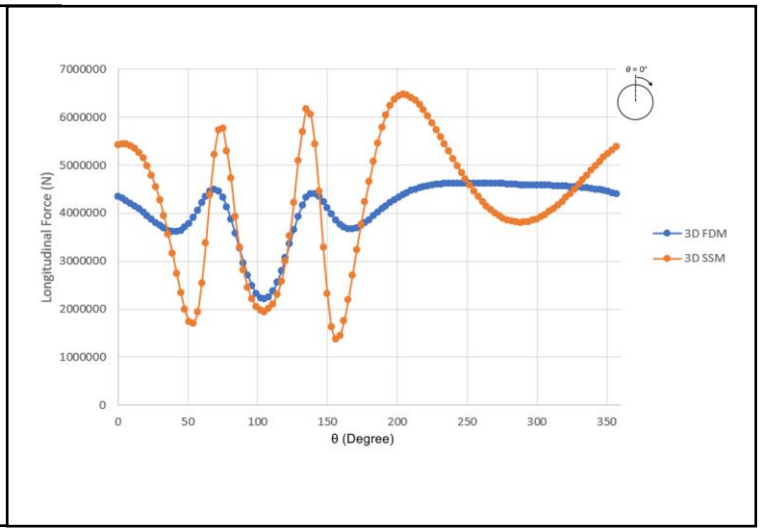

(h) CS 3 Longitudinal force comparison

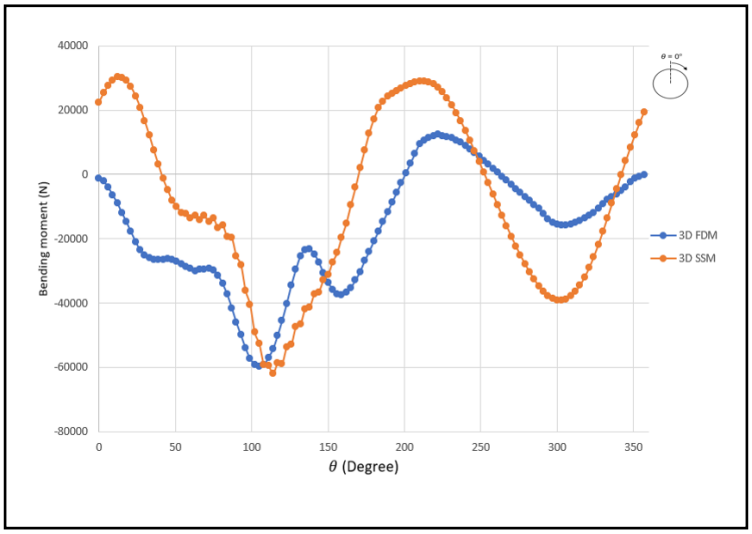

(i) CS 3 Bending moment comparison

Figure 5-3 Comparison of member forces after creation of cross passage opening (continues lining)

CS	R_N^2 for N	$\frac{N_{SSM}}{N_{FDM}}$	R_F^2 for F	$\frac{F_{SSM}}{F_{FDM}}$	R_M^2 for M	M_{SSM}/M_{FDM}
1	0.933	0.953	0.711	1.025	0.974	0.981
2	0.938	1.16	1.714	0.68	0.93	0.83
3	0.73	1.03	0.3523	1.465	0.325	2.33

Table 5-2 Quantitative comparison between the 3D SSM results and 3D FDM results after opening (continues lining).

Based on both graphical and quantitative comparisons, it is evident that the predicted member forces obtained from both models align with each other. Therefore, it can be reasonably concluded that, for similar cases, one can utilize the more straightforward 3D Shell-Spring Models (3D SSMs) to quantify member forces instead of resorting to the more complex 3D Finite Difference Models (3D FDMs). This conclusion underscores the practicality and efficiency of employing 3D SSMs for the assessment of member forces in scenarios with similar characteristics. By opting for the simpler modelling approach, engineers and analysts can potentially save time and resources while still obtaining reliable and accurate results for the evaluation of structural behaviour in tunnel linings with openings.

5.2. Segmental Lining

Figure 5.4 provides valuable insights into the stress distributions in different conditions, considering the effect of circumferential and longitudinal joints. Several observations can be made:

Effect of Joints on Axial Forces: In both cases where the effect of circumferential and longitudinal joints is considered, it's clear that the stress distribution differs from that of a continuous lining. In the continuous lining, axial forces tend to increase at the center of each segment and dip at its end. However, the presence of longitudinal joints interrupts this curvy flow path of axial force.

Longitudinal Forces: In CS1 (A) and CS2 (A), longitudinal forces exhibit very high tensional values between segments, which is not observed in the continuous lining where only compression forces seem to exist.

Bending Moments: Bending moment profiles do not exhibit significant changes in the 3D Finite Difference Model (3D FDM) when compared to the continuous lining. This behavior may be attributed to the intact condition of the ring, which maintains its local stiffness. However, the 3D Shell-Spring Model (3D SSM) shows higher bending values, and the cause of this phenomenon remains unknown. When comparing the two models, it's worth noting that the overall axial force in CS2 (A) tends to agree between both models, but the 3D SSM shows slightly higher peak values. Conversely, the 3D FDM depicts higher peak tensional values in terms of longitudinal forces in

both cross sections. As for bending moments, the 3D SSM tends to exhibit higher peak values compared to the 3D FDM.

In conclusion, while the overall member forces between the two models generally show agreement, there are some differences in the peak values and distribution patterns. These findings underscore the importance of considering the modelling approach and assumptions when analysing the structural behaviour of tunnel linings with openings.

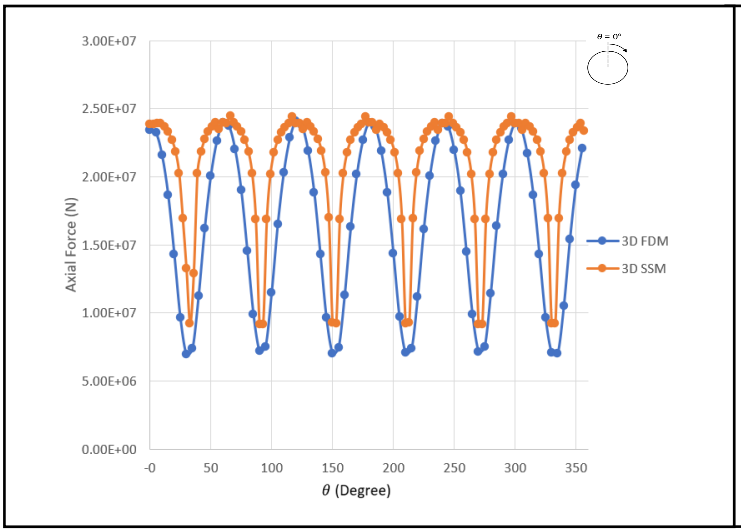

(a) CS 1 Axial force comparison

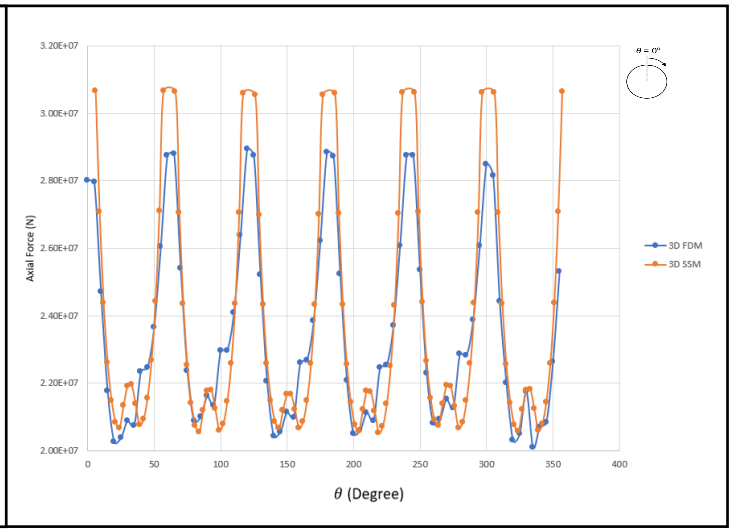

(b) CS 2 Axial force comparison

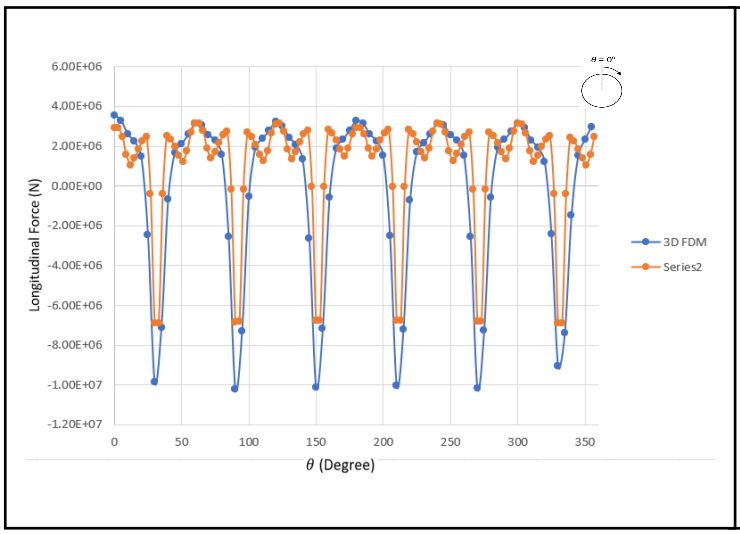

(c) CS 1 Longitudinal force comparison

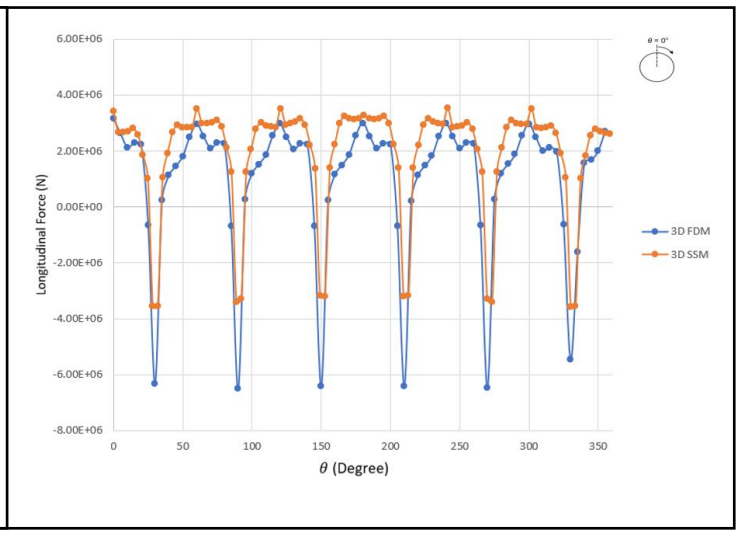

(d) CS 2 Longitudinal force comparison

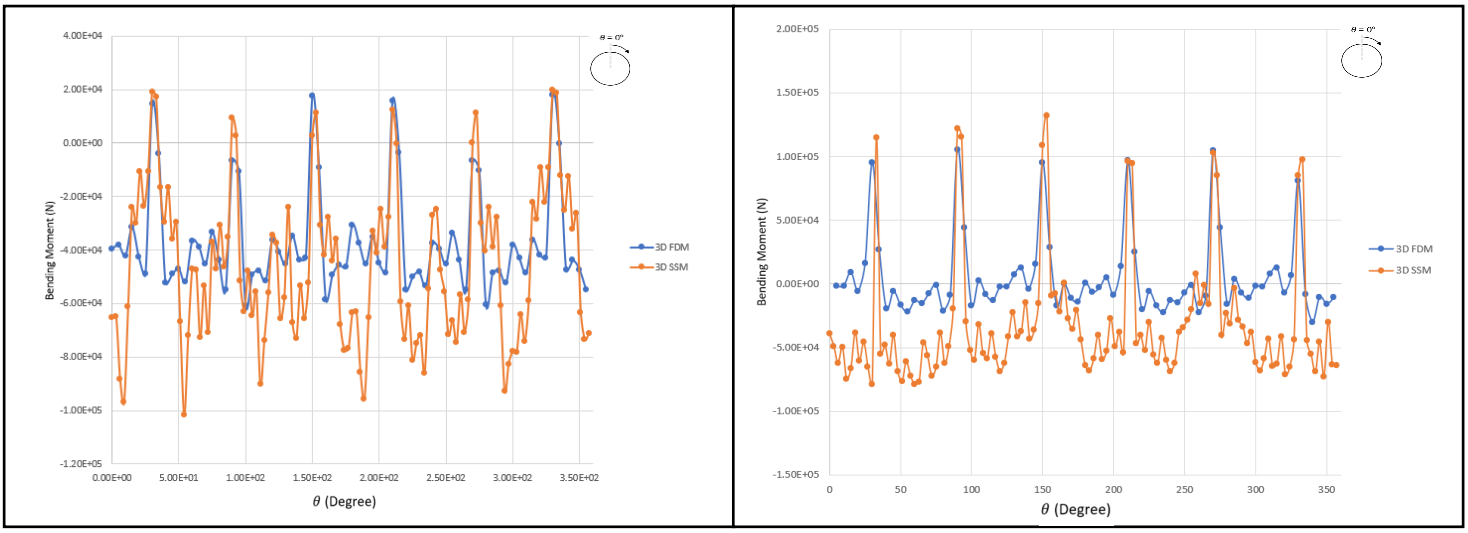

(e) CS 1 Bending moment comparison

(f) CS 2 Bending moment comparison

Figure 5-4 Comparison of member forces before creation of cross passage opening (segmental lining)

CS	R_N^2 for N	$\frac{N_{SSM}}{N_{FDM}}$	R_F^2 for F	$\frac{F_{SSM}}{F_{FDM}}$	R_M^2 for M	M_{SSM}/M_{FDM}
1	-	0.97	0.78	0.698	-	1.32
2	-	1.09	-	57.1	-	-

Table 5-3 Quantitative comparison between the 3D SSM results and 3D FDM results before opening (segmental lining)

quantitative comparison was not possible for most of the section due to differences in the amount of data extracted from the two models.

It's important to note that only one cross section (CS1) was analysed after the creation of the opening, primarily because this section is of utmost importance for designing the temporary support system. This is where the maximum member forces acting in the tunnel lining are typically observed. It was expected that the load transfer behaviour between the opened ring and the unopened adjacent ring would be disturbed due to the presence of longitudinal and circumferential joints. Additionally, it was anticipated that the axial force distribution in the unopened adjacent ring would be reduced as a result of introducing these joints into the calculation. The obtained results in Fig. 5.3 a–f clearly demonstrate that the consideration of longitudinal and circumferential joints in the calculation can significantly affect the stress redistribution induced by the cross-passage opening in the tunnel lining. Therefore, it is essential to incorporate the effects of longitudinal and circumferential joints into numerical or analytical models to accurately simulate the prevailing conditions in the tunnel lining.

In contrast to the 3D Finite Difference Model (3D FDM), the 3D Shell-Spring Model (3D SSM) appears to be a more suitable approach for this purpose due to its simplicity in model creation and the shorter time required for calculations. Furthermore, it's evident from the results that the member forces induced in the segmental lining are considerably high when compared to the undisturbed states of the tunnel lining. This raises concerns about potentially overstressing the segments. As an alternative approach, an interaction diagram can be used to assess whether the induced member forces exceed the structural capacity of the tunnel lining, as shown in Fig. 5.5. The diagram illustrates that the induced axial forces and bending moments indeed exceed the capacity of the segmental ring. This emphasizes the critical importance of implementing a temporary support system during the construction of the cross-passages to ensure the safety and integrity of the tunnel lining.

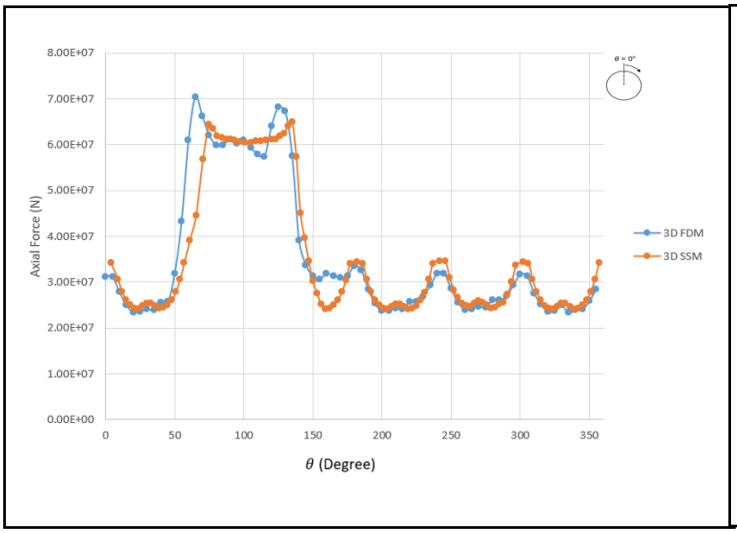

(a) CS 1 Axial force comparison

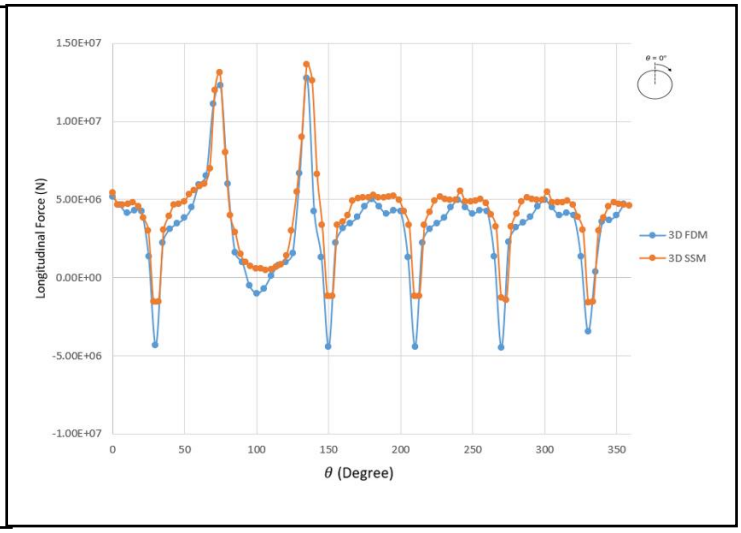

(b) CS 1 Longitudinal force comparison

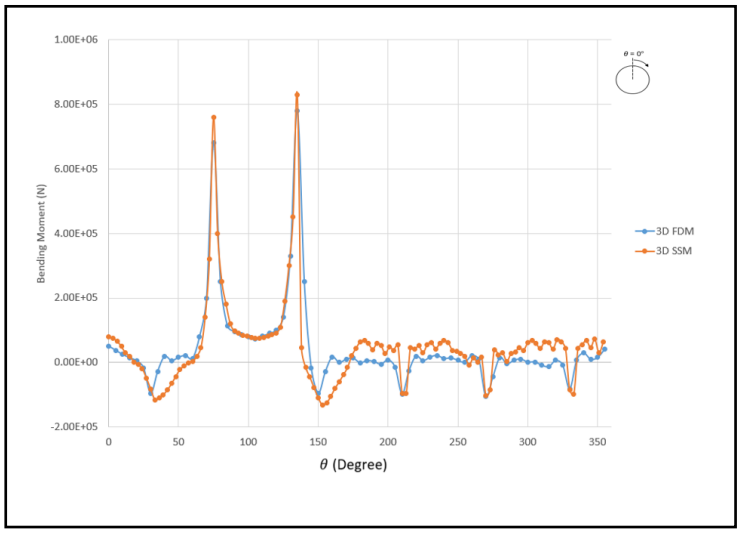

(c) CS 1 Bending moment comparison

Figure 5-5 Comparison of member forces after creation of opening (segmental lining)

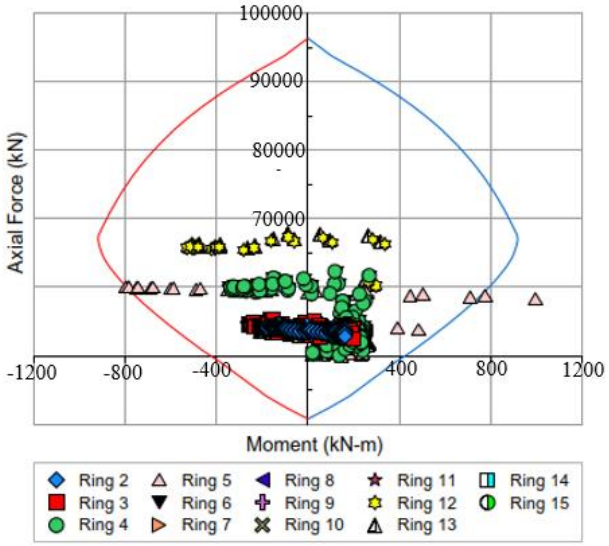

Figure 5-6 Interaction diagram without temporary support system installed.

5.3. Temporary support system

The implementation of a comprehensive temporary support system has had a significant impact on reducing the induced member forces in the tunnel lining, particularly those caused by the formation of openings, as depicted in Figure 5.4. This reduction signifies that the induced axial forces in the segmental lining have effectively transferred to the steel rings, resulting in a decrease in axial force within the segmental lining. Notably, the temporary support system had a more pronounced effect within the 3D Shell-Spring Model (3D SSM) than in the 3D Finite Difference Model (3D FDM), as the reduction in axial forces was more substantial in the former.

To further investigate the enhanced stiffness attributable to the temporary support system, the stiffness of the segmental ring, the steel ring, and the composite lining were calculated using the equations suggested by Yan et al. The calculated stiffness values were 2720.04 MPa/m for the segmental lining and 260.651 MPa/m for the steel support, which results in a composite stiffness of 2980.61 MPa/m.

Based on these calculated values, the installation of the temporary support system has led to a stiffening of the segmental lining by approximately 10%. This increase in stiffness is a crucial aspect of ensuring the structural integrity and stability of the tunnel lining when openings are created during construction.

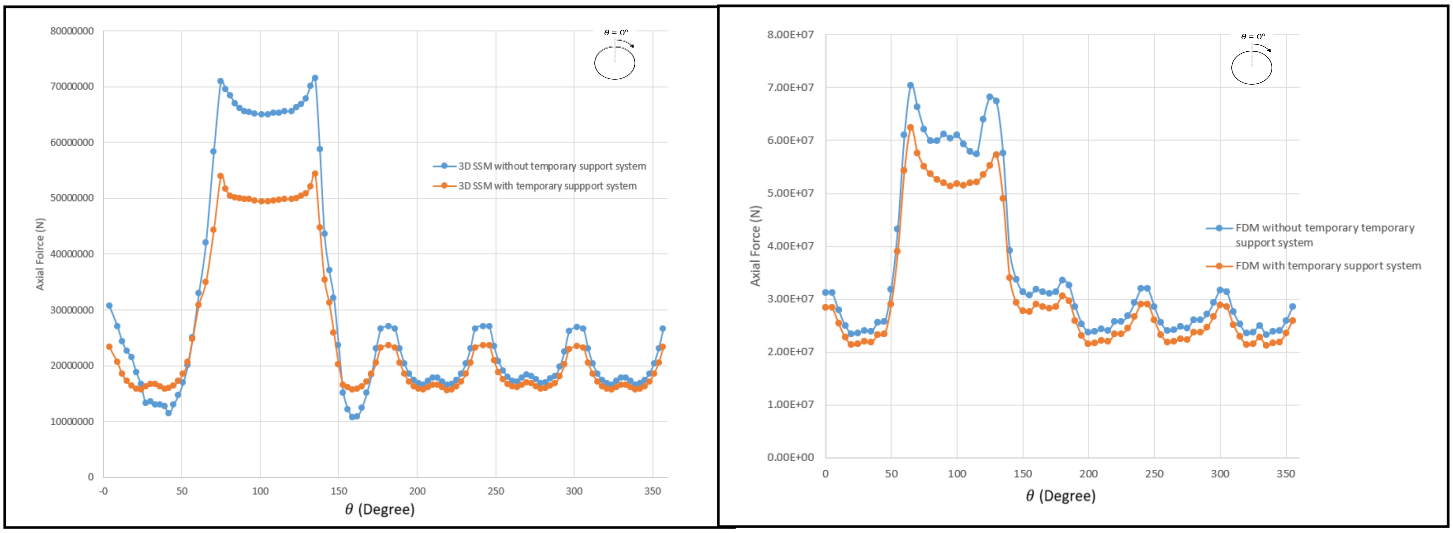

(a) CS 1 Axial force comparison-3D SSM (b) CS 1 Axial force comparison-3D FDM

Figure 5-7 Comparison of member forces after installation of steel support (segmental lining)

Figure 5.6 illustrates that in the 3D Shell-Spring Model (3D SSM), the installation of the temporary support system resulted in a notable reduction in peak axial forces, approximately by 20%. On the other hand, in the 3D Finite Difference Model (3D FDM), the reduction was slightly less, in the order of 13%. This reduction in peak axial forces signifies the effectiveness of the temporary support system in redistributing and mitigating the forces within the tunnel lining when openings are introduced.

Furthermore, an interaction diagram was employed in the 3D SSM to evaluate how the installation of bracings has minimized the risk of the tunnel lining reaching its structural capacity Fig. 5.7. The diagram reveals that, compared to the scenario where bracings were not installed Fig. 5.5, after the adoption of the temporary support system, the segmental rings can now sustain the induced forces without experiencing failure, unlike in the former case. This finding underscores the critical role of the temporary support system in enhancing the safety and structural integrity of the tunnel lining during construction with openings.

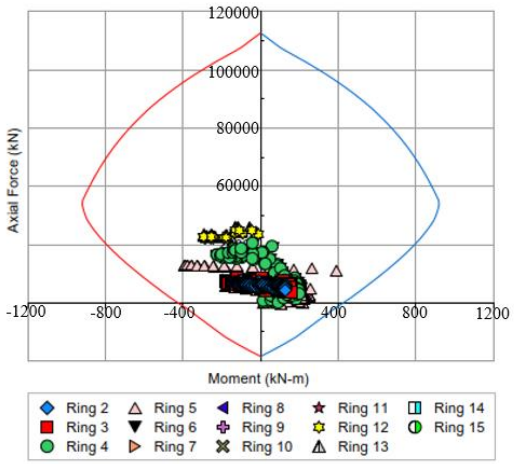

Figure 5-8 Interaction diagram without temporary support system installed.

Based on the comprehensive analysis and findings discussed above, it becomes evident that a temporary support system plays a pivotal and indispensable role in the construction of cross-passages. It serves as a crucial safeguard against overstressing conditions within the tunnel lining when openings are created. As a result, designing an adequate and effective support system becomes of paramount importance in the entire cross-passage design process. Ensuring the safety and structural integrity of the tunnel lining, as well as the overall success of the construction project, hinges on the careful planning and implementation of such a support system. Therefore, engineering and construction teams must prioritize the design and deployment of temporary support systems to mitigate risks and achieve the desired project outcomes.

6. Conclusion

The exploration of stress redistribution in tunnel linings due to cross-passage openings is a critical aspect of tunnel engineering and construction. It involves assessing how the presence of these openings affects the structural integrity of the lining, ensuring that it can withstand the associated loads and continue to provide safe and reliable transport infrastructure.

In this study, we have delved into the analytical methods employed for this assessment, specifically focusing on two approaches: 3D finite difference analysis (3D FDM) and 3D shell-spring analysis (3D SSM). The primary goal was to determine the effectiveness and suitability of each method for evaluating stress redistribution in segmental tunnel linings.

The key findings of this study emphasize the practical advantages of 3D SSMs in this context. These advantages include their compatibility with 3D FDM results, their ability to account for the impact of longitudinal and circumferential joints, and their effectiveness in designing temporary

support systems. Additionally, the 3D SSM approach offers simplicity and precision in quantifying induced loads, making it a valuable tool for engineers and analysts involved in tunnel construction projects.

It's important to note that while fully coupled FDMs offer theoretical accuracy, their computational demands can be prohibitive. As a result, the more streamlined 3D SSM emerges as a practical choice for assessing stress redistribution in tunnel linings with cross-passage openings.

In conclusion, the insights gained from this study provide guidance for engineers and analysts in selecting the most appropriate analytical method for evaluating stress redistribution in tunnel linings. By considering factors such as joint effects and the role of temporary support systems, while also recognizing the advantages of simplified approaches like 3D SSMs, professionals in the field can make informed decisions to ensure the safety and stability of tunnel constructions. This study serves as a valuable contribution to the body of knowledge in tunnel engineering and construction practices.

7. References

Arnau, O., Molins, C., 2011a. Experimental and analytical study of the structural response of segmental tunnel linings based on an in situ loading test. Part 1: numerical simulation Tunneling and Underground Space Technology. 26 (6), 764-777.

Arnau, O., Molins, C., 2011. Experimental and analytical study of the structural response of segmental tunnel linings based on an in situ loading test. Part 2: Numerical simulation. Tunnelling and Underground Space Technology 26, 778–788. https://doi.org/10.1016/j.tust.2011.04.005

Behnen, G., Nevrly, T., Fischer, O. 2015. Soil-structure interaction in tunnel lining analyses Geomechanics and Tunnelling. 38, 96-105.

Do, N.A., Dias, D., Oreste, P., Djeran-Maigre, I., 2014a. Three-dimensional numerical simulation for mechanized tunnelling in soft ground: The influence of the joint pattern. Acta Geotechnica 9, 673–694. https://doi.org/10.1007/s11440-013-0279-7

Do, N.A., Dias, D., Oreste, P., Djeran-Maigre, I., 2014b. Three-dimensional numerical simulation of a mechanized twin tunnels in soft ground. Tunnelling and Underground Space Technology 42, 40–51. https://doi.org/10.1016/j.tust.2014.02.001

Do, N.A., Dias, D., Oreste, P., Djeran-Maigre, I., 2013c. 2D numerical investigation of segmental tunnel lining behavior. Tunnelling and Underground Space Technology 37, 115–127. https://doi.org/10.1016/j.tust.2013.03.008

Do, N.A., Dias, D., Oreste, P., Djeran-Maigre 2D numerical investigation of segmental tunnel lining behavior. https://doi.org/10.1016/j.tust.2013.03.008

H. DUDDECK. Zu den Berechnungsmethoden und zur Sicherheit von Tunnelbauten.Bauingenieur, 47(2):43–52, 1972.

H. DUDDECK. Zu den Berechnungsmodellen f ¨ur die Neue¨OsterreichischeTunnelbauweise (N¨

OT). Rock Mechanics, (Suppl. 8):3–27, 1979.

H. DUDDECK. Empfehlungen zur Berechnung von Tunneln im Lockergestein (1980).Released from Arbeitskreis Tunnelbau, DGEG. Bautechnik, 57(10):349–356, 1980.

H. DUDDECK and J. ERDMANN. Structural design models for tunnels. Tunnelling 82,pages 83–91, 1982.

J. M. DUNCAN and C.-Y. CHANG. Nonlinear analysis of stress and strain in soils. Journal of the Soil Mechanics and Foundations Division ASCE, (96, SM 5):1629–1653, 1963.

M. R. DYER, M. T. HUTCHINSON, and N. EVANS. Sudden valley sewer: a case history.

In R. J. Mair and R. N. Taylor, editors, International Symposium on Geotechnical Aspectsof Underground Construction in Soft Ground, pages 671–676, London, 1996. Balkema.

H. H. EINSTEIN. Improved desing of tunnel supports. Cambridge, Mass.: Massachusetts Institute of Technology, Department of Civil Engineering, 1 to 6, 1979-1980.

H. H. EINSTEIN and C. W. SCHWARZ. Simplified analysis for tunnel supports. Journal ofthe Geotechnical Engineering Division, pages 499–517, 1979.

K. ENGELBRETH. Correspondance on morgan, h.d.: A contribution to the analysis ofstress in a circular tunnel. Geotechnique, 11(3):246 – 248, 1961.

J. ERDMANN. Vergleich ebener und Entwicklung r¨aumlicher Berechnungsverfahren f¨ur Tunnel.

Bericht nr. 83-40, Institut f¨ur Statik, TU Braunschweig, 1983.

Epel, T., Mooney, M., Gutierrez, M., Braun, K., DiPonio, M., Long, N. 2018a. Analysis methodologies comparison of estimated and measured precast segment liner loads developed during construction of twin EPB TBM tunnels in Seattle. In Proc. of World Tunnel Congress 2018.

Frodl, S., 2019. Support structures for segments at the construction of cross passages in different soil conditions. Geomechanik und Tunnelbau 12, 69–81. https://doi.org/10.1002/geot.201800062

Itasca. 2009. FLAC Fast Lagrangian Analysis of Continua, Version4.0. User's manual FLAC Fast Lagrangian Analysis of Continua, Version 4.0. User's manual.

Kim, H.J., Eisenstein, Z., 2006. Prediction of tunnel lining loads using correction factors. Engineering Geology 85, 302–312. https://doi.org/10.1016/j.enggeo.2006.03.001

Yan Q, Li SC, Xie C, Li Y (2018) Analytical solution for bolted tunnels in expansive loess using the convergence-confinement method. Int J Geomech 18:4017124

Ribeiro E, Sousa L (2006) Learning with accidents and damage associated to underground works. In: Geotech risk rock tunnels—sel pap from a course geotech risk rock tunnels, pp 7–39. https://doi.org/10.1201/ 9780203963586.ch2

Mashimo H (2002) State of the road tunnel safety technology in Japan. Tunn Undergr Sp Technol 17:145–152. https://doi.org/10. 1016/S0886-7798(02)00017-2

Lee T-H, Choi T-C (2017) Numerical analysis of cross passage opening for TBM tunnels. In: Proceedings of the 19th international conference on soil mechanics and geotechnical engineering, Seoul, pp 1713–1719

The Professional Standards Compilation Group of People's Republic of China (PSCG PRC) (2004) JTG D70-2004 Code for design of road tunnel. Beijing

ITA COSUF (2019) Current practice on cross-passage design to support safety in rail and metro tunnels

Kuyt J (2015) Observed loading behaviour during cross passage construction: Brisbane Airport Link Project. Colorado School of Mines

Catsman WCGW (2018) Interaction between soil and tunnel lining during cross passage construction using artificial ground freezing. Delft University of Technology

Murray MJ, Eskesen SD (1996) Design and construction of cross passages at the Storebaelt Eastern Railway tunnel. In: Tunnel-ling'97, pp 463–479

Klappers C, Grubl F, Ostermeier B (2006) Structural analyses of segmental lining—coupled beam and spring analyses versus 3D-FEM calculations with shell elements. Tunn Undergr Sp Tech-nol 21:254–255. https://doi.org/10.1016/j.tust.2005.12.116

Zhang Z-Q, Xu J, Wan X-Y (2007) Study on tunnel construction mechanics at intersection of horizontal adit and major tunnel in highway. Yantu Lixue(Rock Soil Mech) 28:247–252

Li Z, Soga K, Wright P (2016) Three-dimensional finite element analysis of the behaviour of cross passage between cast-iron tunnels. Can Geotech J 53:930–945. https:// doi. org/ 10. 1139/ cgj-2015-0273

The British Tunnelling Society and The Institution of Civil Engineers (2004) Tunnel lining design guide

International Tunnelling Association (2000) Guidelines for the design of shield tunnel lining (ITA WG 2 report). Tunn Undergr Sp Technol 15:303–331. https:// doi.org/ 10. 1016/ S0886- 7798(00) 00058-4

Murakami H, Koizumi A (1980) On the behaviour of the trans-verse joints of a segment. In: Proceedings of the Japan society of civil engineers. japan society of civil engineers, pp 73–86

Gall VE, Marwan A, Smarslik M et al (2018) A holistic approach for the investigation of lining response to mechanized tunnelling induced construction loadings. Undergr . Sp3:4560. https://doi.org/10.1016/j.undsp.2018.01.001

Li Z, Soga K, Wright P (2015) Long-term performance of cast-iron tunnel cross passage in London clay. Tunn Undergr Sp Technol 50:152–170. https://doi.org/10.1016/j.tust.2015.07.005

Gruebl F (2012) Segmental ring design—new challenges with high tunnel diameters. TAI J (Half Yrly Tech J Indian Chap TAI) 1:4–9

Brand EW, AS B (1977) Soil compressibility and land subsidence in Bangkok

Balasubramaniam AS, Oh EYN, Phienwej N (2009) Bored and driven pile testing in Bangkok sub-soils. Lowl Technol Int 11:29–36